EVALUATING PRESTRESSING STRANDS AND POST-TENSIONING CABLES IN CONCRETE STRUCTURES USING NONDESTRUCTIVE METHODS

By

Dr. Elin Jensen, Principal Investigator

Dr. Nabil Grace, Co-Principal Investigator

Mr. Samuel Kumi, Research Assistant

Department of Civil and Architectural Engineering
Lawrence Technological University
Southfield, MI 48075-0134

November 2015

TECHNICAL REPORT DOCUMENTATION PAGE

<table>
<tr><td>1. Report No.
RC-1632</td><td>2. Government Accession No.
N/A</td><td colspan="3">3. MDOT Project Manager
Beckie Curtis</td></tr>
<tr><td colspan="2" rowspan="2">4. Title and Subtitle
Evaluating Prestressing Strands and Post-Tensioning Cable in Concrete Structures using Nondestructive Evaluation Methods</td><td colspan="3">5. Report Date</td></tr>
<tr><td colspan="3">6. Performing Organization Code
N/A</td></tr>
<tr><td colspan="2">7. Author(s)
Dr. Elin Jensen, Dr. Nabil Grace, and Mr. Samuel Kumi</td><td colspan="3">8. Performing Org. Report No.
N/A</td></tr>
<tr><td colspan="2" rowspan="3">9. Performing Organization Name and Address
Lawrence Technological University
21000 West Ten Mile Road
Southfield, Michigan 48075</td><td colspan="3">10. Work Unit No. (TRAIS)
N/A</td></tr>
<tr><td colspan="3">11. Contract No.
2010-0293</td></tr>
<tr><td colspan="3">11(a). Authorization No.
Z4</td></tr>
<tr><td colspan="2" rowspan="2">12. Sponsoring Agency Name and Address
Michigan Department of Transportation
Research Administration
8885 Ricks Rd.
P.O. Box 30049
Lansing MI 48909</td><td colspan="3">13. Type of Report & Period Covered
Final Report
10/01/12 to 6/30/2015</td></tr>
<tr><td colspan="3">14. Sponsoring Agency Code
N/A</td></tr>
<tr><td colspan="5">15. Supplementary Notes</td></tr>
<tr><td colspan="5">16. Abstract
The objectives were to evaluate the ability of different NDE methods to detect and quantify defects associated with corrosion of steel reinforcement and grout defects in post-tensioning applications; and to evaluate the effectiveness of selected NDE methods to detect and quantify the deterioration. The study included side-by-side box beam bridges for evaluation of the condition of prestressing strands and web reinforcement. Decommissioned box beams were tested in the laboratory to relate the quantified deterioration to the measured residual flexural capacity. Also a segmental bridge was included for evaluation of the condition of the web reinforcement and post-tensioning ducts. Laboratory specimens simulated debonding and voids around steel reinforcement, loss of cross section area of steel reinforcement, and various grouting challenges. The NDE methods used were 1) ultrasonic testing for delamination/void detection; 2) electrochemical measurements for assessing the corrosive environment; and 3) magnetic flux leakage (MFL) to estimate loss of cross sectional area of embedded steel. Ultrasonic echo-pulse tomography was able to detect debonding of the steel reinforcement and to detect internal voids and delamination. The method was able to quantify the depth of the defect but not the defect length. Electrochemical testing isolated the areas with high chance of corrosion. The MFL pilot demonstration showed that MFL can detect changes in the area of the steel reinforcement in laboratory and field applications. Presently, the calibration overestimates the steel loss. There was good agreement between estimated beam flexural capacity based on NDE results and the measured capacity of full scale box beams.</td></tr>
<tr><td colspan="2">17. Key Words
Corrosion, Concrete, Prestressed, Post-tensioning, Nondestructive testing, ultrasonic testing, magnetic flux leakage, laboratory and field investigation</td><td colspan="3">18. Distribution Statement
No restrictions. This document is available to the public through the Michigan Department of Transportation.</td></tr>
<tr><td>19. Security Classification - report
Unclassified</td><td colspan="2">20. Security Classification - page
Unclassified</td><td>21. No. of Pages</td><td>22. Price
N/A</td></tr>
</table>

DISCLAIMER

The contents of this report reflect the views of the authors who are responsible for the facts and accuracy of the data presented herein. The contents do not necessarily reflect the official views or policies of the Michigan Department of Transportation, nor Lawrence Technological University. This report does not constitute a standard, specification, or regulation. Trade or manufacturer's names, which may appear in this report, are cited only because they are considered essential to the objectives of the report. The United States (U.S.) government and the State of Michigan do not endorse products or manufacturers.

TABLE OF CONTENT

LIST OF FIGURES

LIST OF TABLES

EXECUTIVE SUMMARY

Deterioration of prestressed and post-tensioned concrete members is highly related to the concrete durability and corrosion of the steel reinforcement. In the case of prestressed structures the corrosion causing loss of reinforcement material may also cause localized concrete damage such as cracking, delamination and spalling. For post-tensioned structures the corrosion of the strands is typically associated with voids in the otherwise grouted ducts. Common for both types of reinforcement deterioration is that the onset of corrosion damage occurs without visual signs such as cracks and stains on the concrete surface. Therefore, it is critical to be able to assess the condition of the reinforcement to evaluate the safety of these concrete structures. Detailed condition assessment data afford engineers the ability to make informed decisions to determine short-term as well as long-term maintenance and repair activities. The general consensus among researchers and practitioners is to use multiple nondestructive test methods along with visual inspections and coring to effectively assess the structural performance.

The goal of this study was to assess the effectiveness of multiple nondestructive evaluation (NDE) methods to evaluate the condition of prestressed concrete bridges exhibiting deterioration associated with corrosion of the steel reinforcement. The research plan was designed around an experimental approach and included both laboratory and field investigations. The objectives were to (1) develop laboratory references, for selected NDE methods, for detecting and quantifying defects associated with corrosion of steel reinforcement and grout defects in post-tensioning applications; and (2) evaluate the effectiveness of the selected NDE methods to detect and quantify deterioration in the field using both in service and decommissioned bridges.

Side-by-side box beam bridges were selected for evaluation of the condition of prestressing strands and web reinforcement. Decommissioned box beams were tested in the laboratory to relate the impact of the estimated material deterioration, by the NDE methods, and the measured residual flexural capacity of the beams. Also a segmental bridge was included for evaluation of the condition of the web reinforcement and post-tensioning ducts. Specialized laboratory specimens were designed for this study to simulate debonding and voids around steel reinforcement, loss of cross section area of steel reinforcement, and various grouting challenges. The principal NDE methods used were ultrasonic, magnetic and electrochemical. The following primary methods were used:

- Ultrasonic assessment for delamination, void detection and thickness measurements.
- Electrochemical half-cell potential assessment for assessing the corrosive environment.
- Magnetic flux leakage assessment to estimate loss of cross sectional area of steel reinforcement.

The ultrasonic and the electrochemical assessments were conducted using commercially available systems. The magnetic flux leakage assessment were performed using a strong earth magnet mounted on a mobile unit. The change in magnetic field leakage as the magnet passes over the steel reinforcement is correlated to steel loss. The pilot version of the MFL mobile system was developed at the Center for Innovative Research at Lawrence Technological University.

Ultrasonic echo-pulse tomography was able to detect debonding of the steel reinforcement and to detect internal voids and delamination. The method was able to quantify the depth of the defect but not able to distinguish the debonding length around the reinforcement; unless cracking and delamination had reached an advanced stage. Electrochemical testing isolated the areas with high chance of corrosion. From the field evaluation of the box beams, the areas showing high chance of corrosion coincided with areas experiencing increased ultrasonic reflections indicating various stages of cracking and delamination around the steel reinforcement. The MFL pilot demonstration showed that MFL can detect changes in the area of the steel reinforcement in laboratory and field applications. Presently, the MFL calibration displays the strongest correlation between predicted and actual loss when the loss is spread out over a longer area than when it is concentrated (12 inches contrast to 3 inches). There was good agreement between estimated beam flexural capacity based on NDE assessment and the measured capacity of full scale box beams.

The study proposes an implementation strategy for integrating the use of ultrasonic echo-pulse tomography to detect and quantify defects around the reinforcement. The method is able to evaluate the extent of deterioration along the reinforcement beyond the immediate area suffering from extensive visual deterioration such as rust stains, spalling and cracking. Furthermore, ultrasonic assessment can detect early deterioration in the shear key region of the box beams. The study also proposes the use of electrochemical assessment as part of monitoring the change in the chance of corrosion in areas that exhibit surface cracking developed during construction, early deployment, or other events. The MFL mobile scanner used in this study is not generally field worthy until it is running on tracks mounted on the structure or a scaffold system.

CHAPTER 1: INTRODUCTION

1.1 General

Detailed condition assessment data afford asset managers and structural engineers the ability to make informed decisions to improve short-term as well as long-term maintenance and repair activities of concrete structures. Recent advancements in nondestructive evaluation techniques produce an excellent source of data for an informed decision.

The major cause of deterioration in prestressed strands and post-tension cables in bridges is corrosion of prestressed strands which is usually associated with delamination and spalling as well as grouting defects in post-tensioned ducts which also results in corrosion of post-tensioned cables. It is against this background that a study was conducted to evaluate the condition of prestressing strands and post-tensioning cables in concrete structures using nondestructive evaluation (NDE) methods. The following primary nondestructive methods were deployed: ultrasonic assessment for delamination and void detection; electro-chemical half-cell assessment for detecting corrosive environment; and magnetic flux leakage to determine loss of cross sectional area of rebar and strands.

Three groups of laboratory specimen with simulated defects of voids and cross-sectional area loss were designed for testing using the above nondestructive methods. Three side-by-side field beams from Kent County Road Commission decommissioned after 39 years of service were selected for nondestructive evaluation and residual flexural testing. Field evaluations were also conducted on portions of the segmental bridge carrying US-131 over Muskegon River, 6 miles south of Big Rapids as well as segments of the side-by-side box beam bridge carrying I-96 over Canal Road in Lansing. Results of nondestructive assessment conducted on selected box beams of northbound US-24 over Middle Rouge River have been presented in the Appendix of this report as an additional study.

1.2 Statement of Problems

Prestressed beams commonly used in highway bridge construction and segmental post-tensioned bridges are widely used for medium and long span bridge construction. These types of structures rely heavily on steel prestressing strands and post-tensioning cables for strength and durability. Additionally, it is very important during the construction of these bridges to implement an effective quality control plan to ensure proper placement of the strands and to ensure that the ducts are fully grouted in accordance with the design. Methods to determine the overall conditions of these strands are critical to verify the overall integrity and safety of these structures. Since the strands are embedded in concrete, and often the area is complex and congested, nondestructive evaluation (NDE) methods are needed to assess the condition of these structures. When the evaluation is performed routinely the results can aid the management of the asset in terms of operation, repair and replacement activities.

In particular, exposed structures like highway bridges are more vulnerable to environmental deterioration. The deterioration of prestressed and post-tensioned concrete members is highly related to the concrete durability and corrosion of the steel reinforcement. In the case of prestressed structures the corrosion products may cause localized concrete damage leading to delamination and spalling. In the case of post-tensioned structures the corrosion is typically associated with regions of voids in the otherwise grouted ducts. Yet, common for both types of structures is that the onset of damage occurs without visual clues such as cracks and stains on the concrete surface. However, a significant indicator of the potential for 'hidden' deterioration is the formation of voids. Voids may form either as a result of the corrosion product, delamination and cracks in the prestressed concrete beam, or voids due to lack of proper grouting of the post-tensioning ducts. A second indicator is the change in magnetic resistance of the strands due to the loss of cross section area.

During the last decade, governments and industry have made significant investments into developing new non-destructive testing (NDT) methods for assessing the conditions of prestressed and post-tensioned concrete structures. The Federal Highway Administration's (FHWA) Office of Infrastructure Research and Development has identified NDE as a primary activity in achieving long term infrastructure performance as well as durable infrastructure systems (FHWA-HRT-08-069).

At the present time, the general consensus among researchers and practitioners is to use multiple NDT methods along with visual inspections and coring to effectively assess the structural performance. There are different nondestructive evaluation (NDE) methods for monitoring and instant assessing prestressed and post-tensioned concrete members. The methods range from semi-permanently installed sensors such as Moisture Sensors, Acoustic Emission Sensors (AES) and Micro Electro-Mechanical Sensors (MEMS) to manually operated mobile sensor systems such as Magnetic Flux Leakage (MFL) and Ultrasonic Pulse-Echo Method.

1.3 Motivation

The research team at Lawrence Technological University (LTU) proposed a comprehensive study to investigate and recommend NDE methods for assessing the conditions of prestressed and post-tensioned concrete members. The study included a review of existing use of NDE methods to evaluate the condition of prestressed and post-tensioned strands in concrete structures as well as to verify the proper grouting of post-tensioned ducts in concrete structures. Experimental laboratory and field investigations were performed to evaluate the NDE methods ability to detect and quantify defects. MDOT engineers assisted in defining the selection criteria and the selection of the candidate bridges.

The outcome of these investigations was to provide recommendations on suitable (rapid and flexible) NDE methods to implement as an inspection technique in the bridge inspection protocol for prestressed and post-tensioned concrete bridge systems.

1.4 Study Objectives

The main objectives of this project are as follows:

- Review existing use of NDE methods to evaluate the condition of prestressed and post-tensioned strands in concrete structures, and to verify the proper grouting of post-tensioned ducts in concrete structures.

- Evaluate the effectiveness of NDE methods to evaluate the condition of prestressed and post-tensioned strands in concrete structures and verify proper grouting of post-tensioned ducts in concrete. Detecting and quantifying defects are the primary measures used to evaluate the methods.
- Development of magnetic flux leakage device using the active MFL method.

1.5 Scope of Study

A detailed experimental investigation was designed to address the study objectives. The study utilized laboratory prepared and field specimens tested in the laboratory as well as field inspection on existing structures. Three sets of laboratory specimen and three salvaged box beams received from Kent County Road Commission were evaluated in the laboratory. Two laboratory box beams were constructed according to the geometry stipulated in MDOT Bridge Design Guides 6.65.10A with pre-induced defects to simulate voids created around prestressed strands and post tensioned cables as a result of corrosion by using plastic tubes as detailed in the construction phase. Three laboratory beams were constructed with pre-induced grinding defects covered with plastic tubes to simulate cross-sectional area loss for detection and quantification using ultrasonic assessment and magnetic flux leakage system. Finally, four beams were constructed to simulate grouting defects normally associated with post-tensioned cables.

Field evaluations were also carried out on sections of the following existing bridges in Michigan, US-131 over Muskegon River, southbound 6 miles south of Big Rapids, MI, and segments of S08-55602 of I-96 over Canal Road in Lansing, MI. The primary employed nondestructive evaluation methods were ultrasonic, magnetic flux leakage and electro-chemical half-cell assessments. This report consists of the following chapters:

Chapter (2): This chapter summaries existing use of NDE methods to evaluate the condition of prestressed and post-tensioned strands in concrete structures as well as to verify proper grouting of post-tensioned ducts in segmental concrete structures.

Chapter (3): This chapter presents details of construction of laboratory specimen as well as methodology and testing on existing bridges in this study: US-131 over Muskegon

River, southbound 6 miles south of Big Rapids and segments of I-96 over Canal Road in Lansing.

Chapter (4): This chapter presents the detailed analysis of the test results from the laboratory investigations.

Chapter (5): This chapter presents the detailed analysis of the test results from the field investigations.

Chapter (6): This chapter presents the summary and conclusions derived from this investigation.

Chapter (7): This chapter presents the recommendations derived from this investigation.

CHAPTER 2: LITERATURE REVIEW

2.1 Application of Non-destructive Test Methods for Assessment of Concrete Structures

Many structures are built of prestressed concrete in which prestressing steel wires are put into a permanent state of tension to compensate for the low tensile strength of the concrete. Hence, tensile cracking in the concrete is minimized by ensuring that the concrete is in compression under normal working loads. However, some existing prestressed concrete bridge beams experience deterioration that raises serious concerns about the long-term durability of structures. The major cause of deterioration in prestressed strands in bridges is corrosion. In prestressed concrete structures, the high stress level in the tendons strongly modifies the steel corrosion process. Stress corrosion is characterized by the coupling between the conventional corrosion (pitting attacks in chloride environment) and the steel micro cracking; the latter induced by the high stress level and hydrogen embrittlement (Nürnberger, 2002). Steel micro cracking can lead to the brittle failure of the prestressing steel even at very low corrosion level and under normal service loads (Spaehn, 1977). In such case, there may be no visible warning before tendon failure.

Deterioration of post-tensioned cables in concrete bridges is also a serious concern. The leading cause of corrosion of post-tensioned cables is insufficient grouting of post-tensioned ducts (Mutsuyoshi, 2001). Corrosion is a significant problem in numerous structures and the associated cost is estimated at billions of dollars every year (Singh, 2000).

Unfortunately, corrosion of prestressing steel in both prestressed and post-tensioned concrete members is not visible by indicators such as corrosion stain and concrete cracking during the early stages. When visual signs of corrosion of prestressing steel occur on these members, the corrosion activities would have been in progress for some time and extensive damage could have resulted (Grace and Jensen, 2010).

Nondestructive evaluation techniques are commonly used in the civil engineering field. The recent increased accuracy in detecting a specific type of parameter, such as material quality and defects, is possible due in part to the development of new testing methods, improved data collection and data analysis, as well as the development of user friendly systems. Contrary to destructive methods, nondestructive methods provide information about material properties and structural conditions without compromising the structure and its serviceability. At the same time, it is paramount to select nondestructive test methods that are field worthy and effective, as well as implement routine evaluation schedules of these structures for improved asset management (Ghorbanpoor, 1999).

NDE technologies used for condition assessment of prestressed and post-tensioning systems can be grouped according to their underlying methods (Azizinamini, 2012). These groups are:

- Visual methods
- Magnetic methods
- Mechanical wave/vibration methods
- Electrochemical methods

The following sections briefly presents the common methods used for condition assessment of concrete structures with specific focus on detection and quantification of defects associated with corrosion of reinforcement and concrete deterioration.

2.2 Visual Methods

Visual evaluation is an important assessment in non-destructive testing and it often provides valuable information. Visual characteristics may be due to poor workmanship as well as structural serviceability and material degradation. It aids the engineer to differentiate between the various signs of distress types. Defects that are usually uncovered by visual evaluation are cracks, pop-outs, spalling, delamination, color stains, surface deterioration and lack of uniformity. Considerable details can be collected from visual evaluation to ascertain the suitability of a structures for its intended purpose and identifying the need for follow up in-depth inspection. An engineer carrying out a visual evaluation of a structure should have a good knowledge of applicable structural details, technical specification, past reports of evaluations done, construction records, details of materials used, construction methods as well as dates of construction.

Furthermore, various technologies have extended the capability of visual inspection by using devices like fiberscopes, bore scopes, magnifying glasses and mirrors, portable and permanent video monitoring equipment, and robotic crawlers. Use of these technologies enable visual inspection where direct perspective is impractical; for example, the bore scope provides enhanced ability to inspect the interior portions of post-tensioned ducts for grout voiding and strand corrosion (Azizinamini, 2012).

2.3 Mechanical Wave Methods

The most commonly used mechanical wave techniques are ultrasonic pulse velocity methods, impact methods, and acoustic emission. These methods make use of (small amplitude) mechanical motion that is imposed in a material. However, they differ in the way that the stress waves are generated and on the signal processing techniques that are used (Azizinamini, 2012).

The two main modes of wave propagation in a solid are longitudinal (compression) waves and transverse (shear) waves. In addition, the mechanical surface excitation will generate other tertiary surface waves. The mechanical wave methods discussed in this section are based on the behavior of the compression and the shear waves. The direction of the particle movement in these two independent modes are shown in Figure 2.1. The compression waves moves faster (higher velocity) than the shear waves and therefore, these wave forms are often referred to as the primary and secondary waves, respectively. The typical primary wave velocity for good quality concrete is about 4000 m/s (13,100 ft./sec) and the typically secondary wave velocity is about 2500 m/s (8,200 ft./sec).

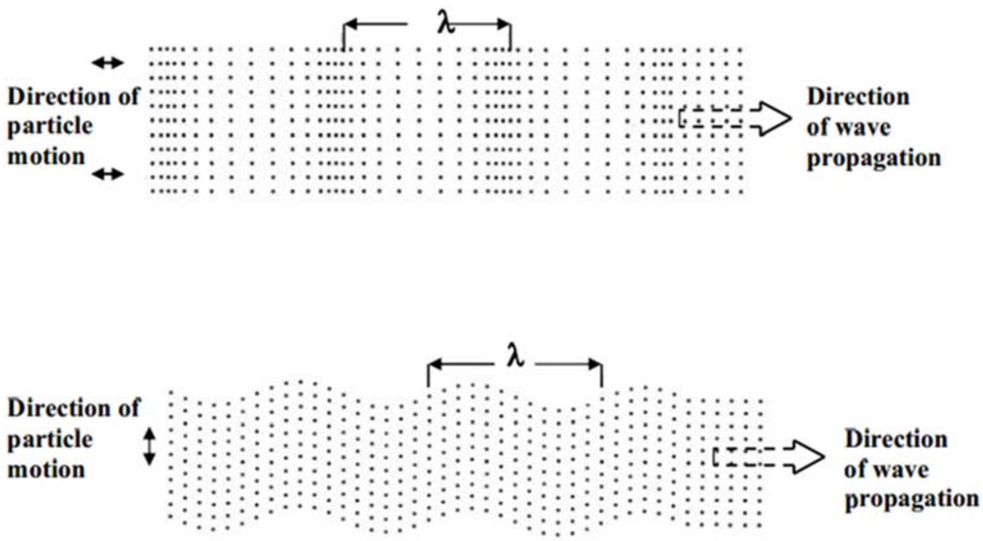

Fig. 2.1: Longitudinal Wave Propagation (Top) and Transversal Wave Propagation (Bottom) (From Ultrasonic Technique for the Dynamic Mechanical Analysis of Polymers, BAM, 2007)

In a homogeneous, isotropic elastic material, the compression wave velocity, V_P, and the shear wave velocity, V_s, can be expressed in terms of the elastic modulus, E, density, ρ and Poisson's ratio, μ.

$$\boldsymbol{V_P} = \sqrt{\frac{\boldsymbol{E(1-\mu)}}{\boldsymbol{\rho(1-2\mu)(1+\mu)}}} \tag{2-1}$$

and

$$\boldsymbol{V_S} = \sqrt{\frac{\boldsymbol{E}}{\boldsymbol{2\rho(1+\mu)}}} \tag{2-2}$$

The mechanical wave technique for thickness and void detection is based on the fundamental concept known as Snell's Law. Assume that a compression (P) wave is imposed on a material with velocity V_1 and the P wave strike an interface with another material with different wave velocity V_2 (e.g. concrete and air). The incident P wave will be reflected and transmitted at the interface as P and S waves, respectively (See Figure 2.2). Snell's law governs the relationships between the angles of the incident, reflected and transmitted waves.

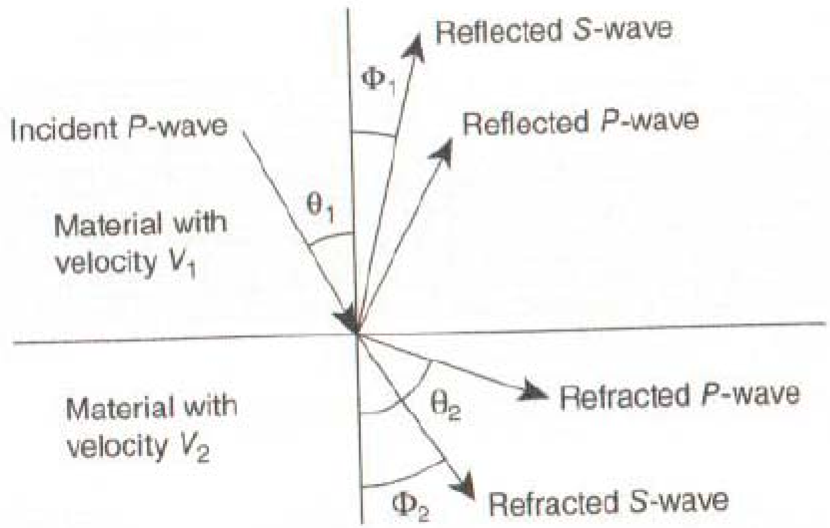

Fig. 2.2: Conversion of a P wave striking an interface between dissimilar materials, following Snell's law (Mehta and Monteiro, 2014)

In addition to the reflection and transmission of waves, the waves in real materials are absorbed and scattered. This phenomena is denoted attenuation. The scattering of waves result from the fact that the propagating medium (like concrete) is not homogenous at the micro level. It contains internal boundaries at which the waves changes abruptly because paste and aggregates have different velocities (elastic properties) (KrautKramer, 1990). Scattering is the reflection of the wave in directions other than its original direction of propagation. Absorption is the conversion of the wave energy to other forms of energy. Therefore, in real materials, the amplitude of the reflected wave is lower than the amplitude of the incident wave.

Generally, a reliable value of attenuation can only be obtained by determining the attenuation experimentally for the particular material being used (NDT Resource Center, 2013). This can be done by varying the frequency during testing, especially at locations where the internal component of the structure is known to compare how best the internal structure matches with the scanned data.

2.3.1 Ultrasonic Testing

Ultrasonic inspections in concrete are used to detect flaws (such as voids) as well as to determine dimensions and material properties (Green, 1987; Bray and McBride, 1992). Ultrasonic inspection consists of sending and receiving waves in materials and measuring the associated travel time of the waves. The wave frequency typically used for concrete structures is in the range of 20 to 150 kHz, however 50 to 60 kHz is suitable for most concrete applications. Low frequencies can be used for very long concrete path lengths and high frequencies can be used for mortars or for short path lengths. High frequency pulses have a well-defined onset but, as they pass through the concrete, become attenuated more rapidly than pulses of lower frequency (International Atomic Energy Agency, Vienna, 2002).

Condition and properties of the test material are determined by analyzing various properties of the sent and received waves. Typical schematics of ultrasonic inspection systems are shown in Figure 2.3 and the configurations are classified as direct and indirect transmission between the transmitter and receiver.

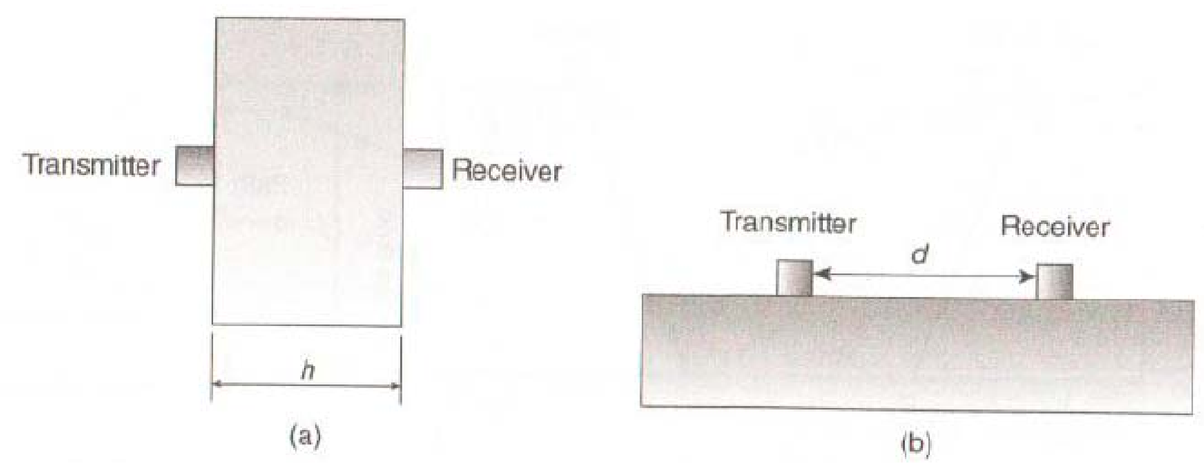

Fig. 2.3: Configuration of a Transmitter and Receiver for (a) Direct and (b) Indirect Transmission (Mehta and Monteiro, 2014)

Several concrete variables can affect the wave velocity in concrete such as level of hydration (porosity), moisture conditions, amount and type of aggregates, micro-cracking and presence of reinforcement (Mehta and Monteiro, 2014). It is important to be aware of the influence of these variables on the results.

Examples of nondestructive testing methods based on the ultrasonic testing principle are pulse velocity, ultrasound pulse echo, impact echo, and acoustic emission. They are based on the principle of sending and receiving waves in a material where condition and properties of the test material are determined by analyzing various properties of the sent and received waves. The methods differ in the way that the stress waves are generated and on the signal processing techniques that are used.

2.3.1.1 Pulse Velocity Test

Pulse velocity testing is based on measuring the travel time of the compression wave between the transmitter and receiver. The direct transmission method is preferred in pulse velocity testing with sensors placed on either side of the concrete and immediately opposite each other (see Figure 2.3). The pulse generated by the transmitter causes waves of several modes but only the travel time of the fastest traveling wave form, the compression wave, is measured. The contact between the concrete and transmitter/receiver is ensured using a liquid coupling material such as cellulose paste. (International Atomic Energy Agency, 2002). A schematic of the pulse velocity system is shown in Figure 2.4.

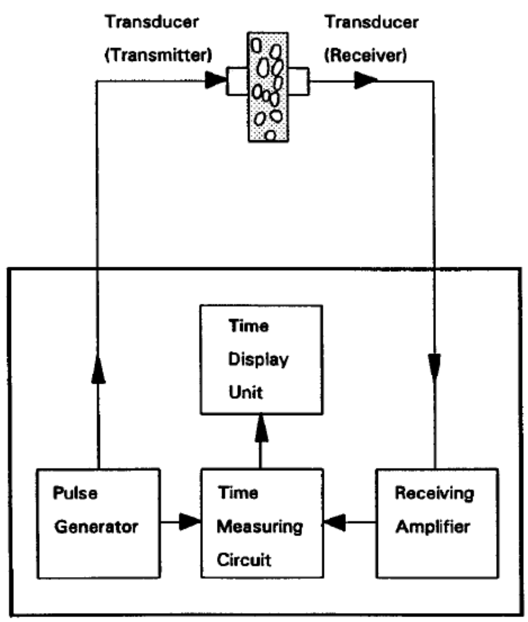

Fig 2.4: Schematic of pulse velocity device (Crawford, 1997)

The pulse velocity, V, is given as the simply ratio of path length, L, of the wave divided by the time, T, it takes for the wave to traverse that path length as shown in equation 2-3

$$V = \frac{L}{T} \qquad (2\text{-}3)$$

Pulse velocity testing is primarily used to determine:

- the uniformity of the concrete expected to have the same properties
- any concrete property changes over time
- the concrete quality by correlating the pulse velocity and the concrete strength
- the elastic properties (elastic modulus and Poisson's ratio)

It is challenging to determine defects using the pulse velocity testing. When compression wave strikes the interface between concrete and air, defects larger than the width of the transmitter/receiver as well as longer than the wavelength of the compression wave may be detected. In general, defects larger than about 4 inches (100 mm) can be detected (International Atomic Energy Agency, 2002).

2.3.1.2 Ultrasound Pulse Echo

Ultrasound pulse echo testing can be used to detect objects, interfaces, and anomalies. A major advantage is the application of the indirect setup requiring only a one sided access to the concrete surface. If the wave velocity, *V*, is known, the wave travel time, *t*, between the transmitter, defect and receiver is used to directly estimate the depth of the defect, *d*. The depth of the defect from the surface of the concrete as shown in equation 2-4:

$$d = \frac{V}{2\,t} \tag{2-4}$$

The illustration in Figure 2.5 shows the transmitted and reflected wave path. This reading is denoted as A-scan. The method is also denoted pitch-catch method.

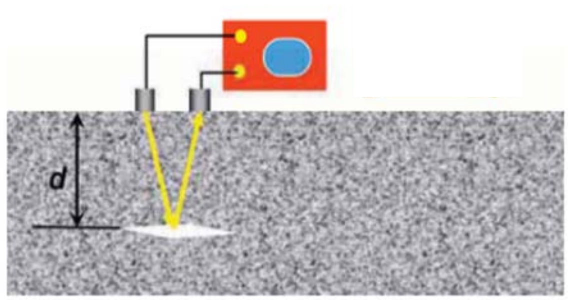

Fig 2.5: Illustration of the Basis of Ultrasonic Pulse Echo Method

(From NDT Systems catalog, Germann Instrument, 2010)

Ultrasound Pulse Echo testing is often conducted at an ultrasound frequency of 50 kHz because of the scattering of the sound waves by the aggregates and air pores (Nead et al, 2013). Care should be taken during testing and analysis with the adjustment of the measuring frequency to reduce the amount of attenuation.

It is recommended to use an array of a minimum of 10 transducers (transmitter/receivers) when using this method for thickness assessment. A mathematical method is used to determine the true depth by use of a phase shift superposition technique to determine the maximum synthetic echo.

The ultrasound pulse echo is capable of assessing defects in concrete elements, debonding of reinforcement bars, shallow cracking, and delamination. The method was also successfully used in the detection of material interfaces, based on phase evaluations of the response. Examples include the interfaces between concrete and steel (e.g., reinforcement) or concrete and air (e.g., grouting defects) (Taffe and Wiggenhauser 2006; Afshari et al. 1996; Krause et al. 2008; Hevin et al. 1998). Very shallow flaws may remain undetected because the surface waves mask the needed compressional or shear-wave signals. Also, as ultrasonic pulse echo works with lower frequencies, some of the defects might remain undetected (Nead et al, 2013).

Investigating ducts is sometimes complicated, in particular for structures with thick concrete cover greater than 4 inches (100 mm). Comprehensive analysis of many A-scan readings, using 3D SAFT (Synthetic Aperture Focusing Technique), produces a 3D topography image and the position of the duct and potential voids can be identified.

2.3.1.3 Impact-Echo

The impact echo (IE) method is a seismic or stress wave–based method used in the detection of defects in concrete, primarily delamination (Sansalone and Carino 1989). The objective of the method is to detect and characterize wave reflectors or “resonators” in a concrete. This is achieved by striking the surface of the tested object and measuring the response at a nearby location (Nead et al, 2013).

The concrete surface is struck (e.g. steel balls), and the response is measured by a nearby contact or air-coupled sensor. The position of the defects or reflectors is obtained from the frequency spectrum of concrete's response to an impact (Nead et al, 2013).

This is an effective method of locating defects in piles, caissons, and plates. A mechanical impact produces stress waves of 1 to 60 kHz. The wavelengths from 50 mm to 2000 mm propagate as if in a homogeneous elastic medium. The mechanical impact on the surface generates compression, shear and surface waves. Internal interfaces or external boundaries reflect the compression and shear waves. When the waves return to the surface where the impact was generated, they can be used to generate displacements in a transducer and subsequently, a display on a digital oscilloscope.

The transducer acoustically mounted on the surface receives the reflections created from the energy impact. The amplitude spectrum is then analyzed to determine if any discontinuities are present (Pessiki et al, 2010**).** Figure 2.6 illustrates the basis of the IE method.

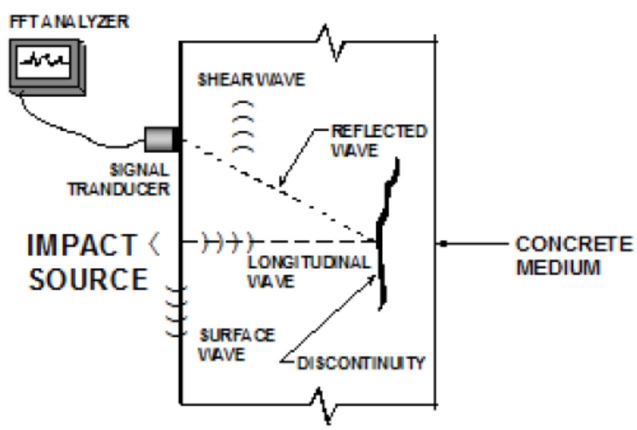

*Figure 2.6: Illustration of the Basis of the IE method. (Pessiki et al, 2010***)**

2.3.2 Acoustic Emission

Acoustic emission is based on analyzing the response of the material during crack propagation. The above discussed stress wave methods are different in that they are based on analyzing the response of the material when subjected to a known signal.

Acoustic Emission (AE) is defined as the elastic energy released from materials which are undergoing deformation and crack propagation. The rapid release of elastic energy, the AE event, propagates through the structure to arrive at the structure surface where a transducer is mounted. These transducers detect the displacement of the surface at different locations and convert it into a usable electric signal. By analysis of the resultant waveform in terms of feature data such as amplitude, energy and time of arrival, the severity and location of the AE source can be assessed (Hellier, 2001).

The main problem in field application is to distinguish the emission caused by defects from ambient emissions. Only breaks occurring after the installation of equipment can be detected. For passive monitoring, vibration sensors are strategically mounted on structural members. These vibration sensors are monitored to “listen” for fracture events due to corrosion of wire strands in the tendons (Azizinamini et al, 2012). Furthermore, severe attenuation of elastic waves in strands bonded with concrete substantially reduces the method's effectiveness (Ciolko et al, 1999).

2.4 Magnetic Methods

Magnetic methods make use of the interaction between magnetic (and associated electric) fields and their interaction with matter. The magnetic based cover meters have been widely used in the concrete industry for locating the steel reinforcement and to determine the concrete cover over the reinforcement. In the last decades the application of the magnetic flux leakage (MFL) method has been further developed to include the estimation of loss of steel reinforcing cross section area due to corrosion (Azizinamini, 2012). While this is a very promising technique that would allow the engineer to quantify reinforcement loss, standardized equipment is not readily available.

2.4.1 Magnetic Flux Leakage (MFL)

The use of MFL for inspecting steel in prestressed concrete members was studied by Kusenberger and Barton (1981) and Sawade and Krause (2007) and was later extended to other on-site inspections (Grosse 2007). Ghorbanpoor et al (2000) developed an MFL sensor using permanent magnets to magnetize steel components in concrete and used the amplitude of detected MFL signals to determine empirically the flaw volume. DaSilva et al. (2009) also reported the use of MFL to estimate the amount of material loss of corroded steel strands in concrete. Studies performed have also shown that the methodology for detecting corrosion in post-tensioned concrete bridges is promising (Ghorbanpoor et al, 2000).

Instrumentation development has been subjected to evaluation and upgrade over the years. Various data analysis techniques have been developed to aid the interpretation of relevant test results. Flaws were recognizable when the flaw size was larger than approximately 10 percent of the cross-sectional area of the specimen. With flaws smaller than 10 percent of the cross sectional area, the correlation method, a signal analysis method based on the correlation concept was shown to be effective (Ghorbanpoor et al, 2000). A study comparing residual magnetic field measurements to magnetic flux leakage measurements, as a method to detect broken prestressing steel, was conducted by Makar et al (2001). According to this investigation, analyses of two and three dimensional magnetic field plots show that the residual magnetic field technique is capable of detecting corrosion of a single wire in a seven-wire strand embedded in concrete with a maximum concrete cover of 2.5 inches. MFL method has been used in Germany and reported that the parameters associated with fractured wires are quantitatively identifiable in the laboratory (Scheel et al, 2003). They also reported application of the method in the field.

Magnetic flux leakage for assessing condition of steel in concrete structures utilizes the ferromagnetic property of the steel to detect disturbance of an externally applied magnetic field due to the presence of flaws in the steel. If the direction of the applied magnetic field is set to be collinear with the longitudinal prestressing steel, the flux lines will also be collinear with the steel elements in the concrete. Any change in cross sectional area of the steel at any point will cause a flux leakage, where the continuous flux lines within the steel will be forced into the medium surrounding the flaw as shown in Figure 2.7. Since the effect of concrete on magnetic field is negligible, the field leakage may be measured by Hall sensors in the air near the surface of the concrete. If the magnetic source and sensors are moved along the length of the concrete member, the changes in the field, due to the presence of flaws in steel, can be recorded as continuous in terms of time and the field amplitude. This is then analyzed to obtain information relevant to the location and extent of the flaw in the steel (Ghorbanpoor, 1999).

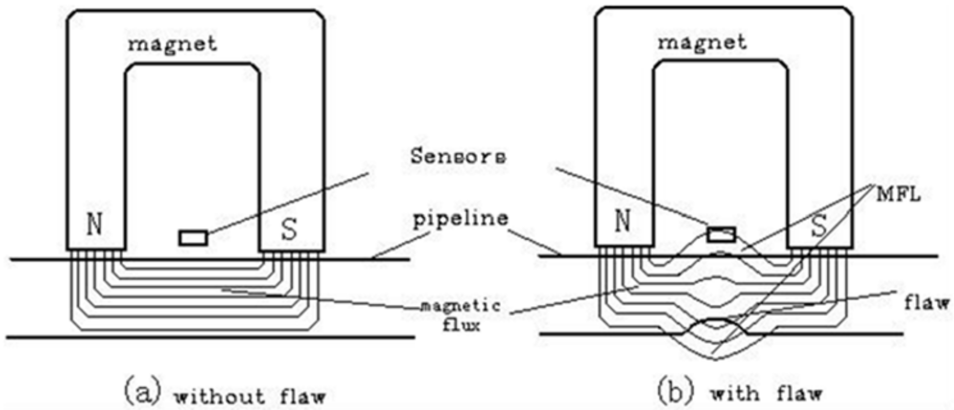

Fig 2.7: Change in magnetic flux before and after detection of flaw (ndt.net)

Magnetism is caused by the presence of molecular current loops, which is caused by two phenomena: the motion of electrons within the atoms and the spin direction of the electrons within the magnet material. In the presence of a magnetic field, a moving charge has a magnetic force exerted upon it. The relationship that governs the force on moving charges through a magnetic field is called Faraday's Law and implies that as a charge q moves with a velocity **V** in a magnetic field **B,** it experiences a magnetic force **F.**

$$F = qVB \qquad (2\text{-}5)$$

where:

F	is magnetic force (newton)
q	is charge (coulomb)
V	is velocity (meter/second)
B	is applied magnetic field (weber/sq. meter)

When a magnetic field comes near ferromagnetic (steel) material, the magnetic flux lines will pass through the steel bar because the steel offers a path of least resistance due to high magnetic permeability compared to the surrounding air or concrete. When discontinuities of defects (corrosion) are present, this low resistance path becomes blocked and the remaining steel may become saturated, forcing some of the flux to flow through the air. Total saturation is not required for detection as orientation of the magnetic field can be altered by even small levels of corrosion. However, there is a saturation level at which all dipoles are aligned and no further alignment is possible. At saturation level, the following relationship is valid:

$$B = \mu H \quad (2\text{-}6)$$

where:

B is Magnetic flux (weber/sq. meter)

μ is Magnetic permeability of the material (weber/ampere meter)

H is Magnetic field strength (ampere/meter)

To use the concept of MFL as a non-destructive evaluation (NDE) tool, the device must have the ability to measure changes in the path of magnetic field force lines near a ferromagnetic material. Such changes in the components of the flux can be detected by one or more sensors and can be analyzed to determine the extent or severity of the flaw. Hall-effect sensors are often used to detect and measure MFL. The sensors are made with semi-conductor crystals that when excited by a passage of current perpendicular to the face of crystal, react by developing a voltage difference across the two parallel faces. The possibility of fabrication of those sensors at any size allows the detection of small flaws on the steel (DaSilva et al, 2009)

There are two primary methods for detecting these field anomalies: active and residual. In the active method, the sensors are placed between the poles of the magnet and readings are obtained as the device is passed over the specimen. In the residual system, the specimen is first magnetized; it is important that the strands become magnetically saturated. Then the device is passed over to read the residual magnetic field. Active MFL is appropriate when large areas of corroded regions exist inside the ducts. However, when the corroded area is small, active MFL is no longer effective (Marcel et al, 2009). An illustration of magnetic flux leakage method is shown in Figure 2.7.

2.4.2. Ground Penetrating Radar

Ground Penetrating Radar (GPR) is a pulse method for locating structural defects (voids and delamination), location of steel reinforcement, pavement layer thickness and structural changes (Loizes et al, 2006; Mehta and Moneteiro, 2014). GPR system is based on the concept of sending an electromagnetic pulse through an antenna to the concrete surface of the testing specimen and then recording the reflected pulses from the internal interfaces, where there is a variation in the dielectric properties (AL-Qadi et al, 2005). It is this reflection phenomenon that allows radar images to be created. A wide range of signal frequencies are used for various practical applications ranging between 50 MHz and 2.5 GHz. Generally, for inspection of concrete structures, antennas with frequencies of 1 GHz are used (Hugenschmidt, 2002; Mehta and Monteiro, 2014).

2.4.2.1 Physical Principle

The two most important factors affecting the propagation of radar pulses in any material are the electrical conductivity and the dielectric constant (Sarrakento, 1997). The behavior of a beam of electromagnetic (EM) energy as it hits an interface between two materials of dissimilar dielectric constants, has been shown in Figure 2.8. Part of the energy would be reflected and the remaining goes through the interface into the second material. The intensity of the reflected energy, AR, is related to the intensity of the incident energy, AI, by the following relationship:

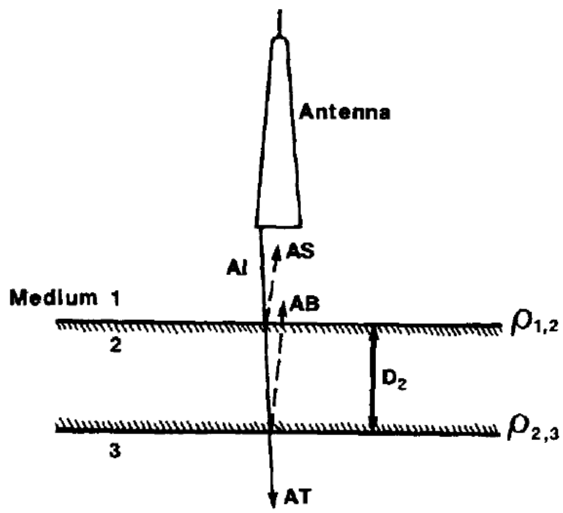

Fig 2.8: Propagation of EM energy through dielectric boundaries.
(International Atomic, Agency, 2002)

$$\mu_{1,2} = \frac{AR}{AI} = \frac{n_2 - n_1}{n_2 + n_1} \qquad (2\text{-}7)$$

where

$\mu_{1,2}$: the reflection coefficient at the interface

n_1/n_2: the wave impedance of materials 1 and 2, respectively, in ohms

or written in terms of dielectric constants, ε_{r1} and ε_{r2}, of material 1 and 2 respectively:

$$\mu_{1,2} = \frac{(\sqrt{\varepsilon_{r1}} - \sqrt{\varepsilon_{r2}})}{(\sqrt{\varepsilon_{r1}} + \sqrt{\varepsilon_{r2}})} \tag{2-8}$$

This gives an indication that when a beam of electromagnetic energy hits the interface between two media of different dielectric constants, the amount of reflection $(\mu_{1,2})$ is determined by the values of their relative dielectric constants. The dielectric constant is strongly affected by the water content and also several other factors such as mix proportions, porosity, pore fluid solution and shapes of particles and pores.

The result of a GPR relief is a radar gram. The radar technique allows to establish the number, position and diameter of all steel bars existing in a surveyed structure and it also allows to locate possible cavities in both reinforced concrete structures and masonry structures. The electromagnetic impulse technique offers the advantage of portable equipment and the capability to detect rapidly large areas from one surface in a completely non-destructive and non-invasive way. One of the main difficulties with the use of GPR is that the results are very difficult to interpret and a skilled technician must be required to produce a reliable end result (Bungey et al, 2003).

2.4.2.2 Application

Locating of reinforcing bars in concrete is one of the most widespread applications of GPR in civil engineering (Ulriksen, 1982). Recently, GPR is also used to locate ducts in post-tensioned bridges. However steel ducts completely reflect the radar signal since they are conductive, so that the tendon breaks or grout defects inside the duct cannot be detected (Pollock et al, 2008). GPR has the potential to monitor grout conditions within non-conducting (plastic) ducts. In particular, GPR is likely sensitive to the occurrence of soft, non-setting and chalky grout or cases of water intrusion due to the changes in dielectric constants and hence reflection (Azizinamini et al, 2012).

2.5 Electrochemical Methods

These methods are used to monitor active corrosion in concrete structures by making use of the electrochemical basis of the process. These approaches offer potential to measure meaningful data related to active corrosion of strand. Most electrochemical techniques use the same measurement set up. It consists of a reference electrode, a working electrode, a counter electrode, and a volt meter. A closed electrical circuit is always required and direct electrical connection to the steel reinforcement must be established as shown in Figure 2.9 (Azizinamini, 2012).

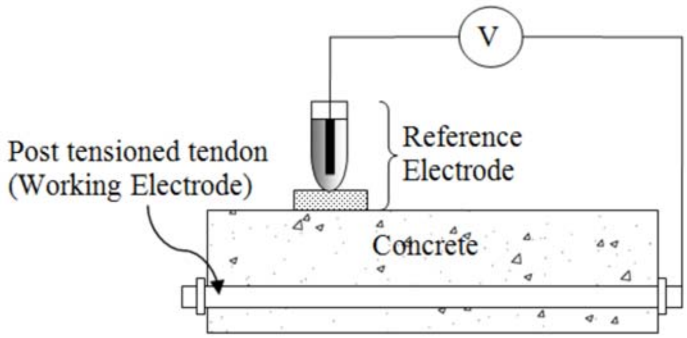

Fig 2.9: Setup for electrochemical techniques (Azizinamini and Gull 2012)

Two non-destructive techniques are commercially available based on the electrochemical process. These are half-cell potential and polarization resistance. The former gives information on the probability of corrosion and the latter is related to the corrosion rate. The half-cell potential measurement is practically and widely employed to identify the presence of corrosion.

2.5.1 Half-cell Potential

The half-cell potential (HCP) measurement is a well-established and widely used electrochemical technique to evaluate active corrosion in reinforced steel and prestressed concrete structures. The method can be used at any time during the life of a concrete structure and in any kind of climate, provided the temperature is higher than 2°C (Elsener, 2003). Half-cell measurements should be taken on a free concrete surface, because the presence of isolating layers (asphalt, coating, and paint) may make measurements erroneous or impossible. Generally, the potential difference between the reinforcement and a standard portable half-cell, using a $Cu/CuSO_4$ standard reference electrode, is measured when the electrode is placed on the surface of a reinforced concrete element. When the reference electrode is shifted along a line or grid on the surface of a member, the spatial distribution of corrosion potential can be mapped (Baumann 2008; Gu and Beaudoin 1998).

Using empirical comparisons, the measurement results can be linked to the probability of active corrosion. Furthermore, it is meaningful to assess the change in potential over a larger surface area to assess if there is an increased chance for an active corrosion cell.

2.5.1.1 Physical Principle

The procedure for measuring half-cell potentials is comparatively straight-forward. A good electrical connection is made to the reinforcement, an external reference electrode is placed on the concrete surface and potential readings are taken on a regular grid on the free concrete surface. Different microprocessor-controlled single or multiple electrode devices have been developed and are commercially available. The best way of representing the data has found to be a color map of the potential field and contour plot, where every individual potential reading can be identified as a small square. Alternatively, frequency plot can be used as well.

Electro-chemical half-cell potential mapping is used to identify localized corrosion of reinforcement which greatly improve the quality of condition assessment of concrete structures (ASTM C 876, Elsener 1992 & 2001, and Cairns and Melville, 2003, Pradhan and Bhattacherjee, 2009). Electrons flow through the steel to the cathode, where they form hydroxide (OH^-) with the available water and oxygen. This creates a potential difference that can be measured by the half-cell method. A schematic view of the electric field and the current flow on steel in concrete is presented in Fig 2.10. Table 2.1 shows interpretation of half-cell potential values as per ASTM C876.

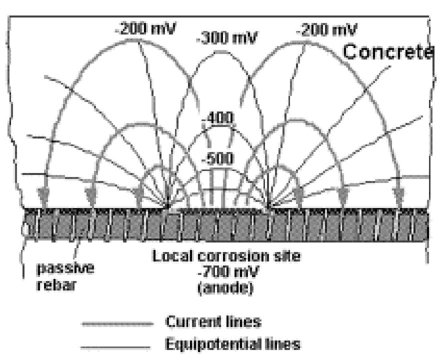

Fig 2.10: Schematic view of the electric field and current flow of an active/passive macro-cell on steel in concrete (Elsener 2001)

It is often necessary to use other data such as chloride contents, depth of carbonation, delamination survey findings, rate of corrosion results and environmental exposure conditions, in addition to corrosion potential measurement to formulate conclusions concerning corrosion activity of embedded steel and its probable effect on service life of a structure. (ASTM Designation: C876-09, Standard test method for corrosion potential of uncoated reinforcing steel in concrete)

Table 2.1 Interpretation of half-cell potential values as per ASTM C876

Half-cell potential (mV) relative to $Cu/CuSO_4$	Chance of rebar being corroded
< -500	Visible evidence of corrosion
-350 to -500	95%
-200 to -350	50%
> -200	5%

Typical order of magnitude for the half-cell potential of steel in concrete measured against a $Cu/CuSO_4$ reference electrode (RILEM TC 154-EMC) is presented in Table 2.2. It is to be noted that Table 2.1 should not be used in isolation, but should be used considering the environmental conditions of the concrete being tested, as this has an impact on the half-cell potential value as shown in Table 2.2.

Table 2.2 Half-cell potential for different types of concrete

Concrete condition	Half-cell potential
Water saturated concrete without O_2	-1000 to -900 mV
Moist, chloride contaminated concrete	-600 to -400 mV
Moist, chloride free concrete	-200 to +100 mV
Moist, carbonated concrete	-400 to +100 mV
Dry, carbonated concrete	0 to +200 mV
Dry, noncarbonated concrete	0 to +200 mV

The main disadvantage of this method is that the potentials measured are too sensitive to moisture content, thickness of concrete cover, surface coating, resistivity of concrete, and the type of electrode (Misra and Uomoto, 1990).

Theoretical considerations and practical experience on a large number of structures have shown (Elsener et al, 1990, 1992 & 1979) that the results of potential mapping on existing structures need careful interpretation. No absolute values of potential can be applied to indicate corrosion hazard in a structure. Depending on concrete moisture content, chloride content, temperature, carbonation of the concrete and cover thickness, surface coating, resistivity of concrete, type of electrode, different potential values indicate corrosion of the rebar on different structures. After repair work, interpretation of half-cell potentials can be even more difficult because alkalinity, composition and resistivity of the pore solution in the repaired areas can be greatly altered compared to the old existing concrete.

2.6 Summary

This chapter highlighted some of the most commonly used nondestructive testing method used for condition assessment of steel reinforced concrete structures. The discussion was limited to topics of visual inspection, mechanical wave methods, magnetic methods, and electrochemical methods. The following basic principles governing the methods were briefly discussed as well as associated applications.

- Visual inspection is for surface evaluation of delamination, cracking, and stains.
- Mechanical wave method is for detecting voids, defects as well as material interfaces.
- Magnetic methods are for locating steel reinforcement and estimating the cross-sectional loss of steel reinforcing material
- Electrochemical methods are for assessing the chance for corrosive environment in reinforced concrete.

CHAPTER 3: EXPERIMENTAL INVESTIGATION

3.1 Introduction

The experimental investigations were undertaken to evaluate the effectiveness of nondestructive evaluation (NDE) methods to assess the condition of prestressed and post-tensioned strands in concrete structures and verify proper grouting of post-tensioned ducts in segmental concrete structures. The study utilized laboratory prepared and field specimens tested in the laboratory as well as field inspection on existing structures. Three sets of laboratory specimen and three salvaged beams received from Kent County Road Commission were evaluated in the laboratory. Specimen 1 was made up of two (2) box beams constructed according to the geometry stiputed in MDOT Bridge Guide section 6.65.10A. The box beams were simulated with voids created around prestressing strands and transverse reinforcement using plastic tubes as detailed in section 3.2.3 of this report. Specimen 2 was made up of two (2) beams constructed with reinforcement simulated with grinding defects to depict cross- sectional area loss as detailed in section 3.3.1, for detection and quantification using ultrasonic and magnetic flux leakage assessments. Specimen 3 was made up of four (4) beams constructed with post-tensioned ducts simulated with grouting defects as detailed in section 3.4.1 to be assessed using ultrasonic method. Laboratory prepared specimen are shown in Figures 3.1 through 3.3.

Figure 3.1: Specimen 1 Box Beams, S1-1 and S1-2.

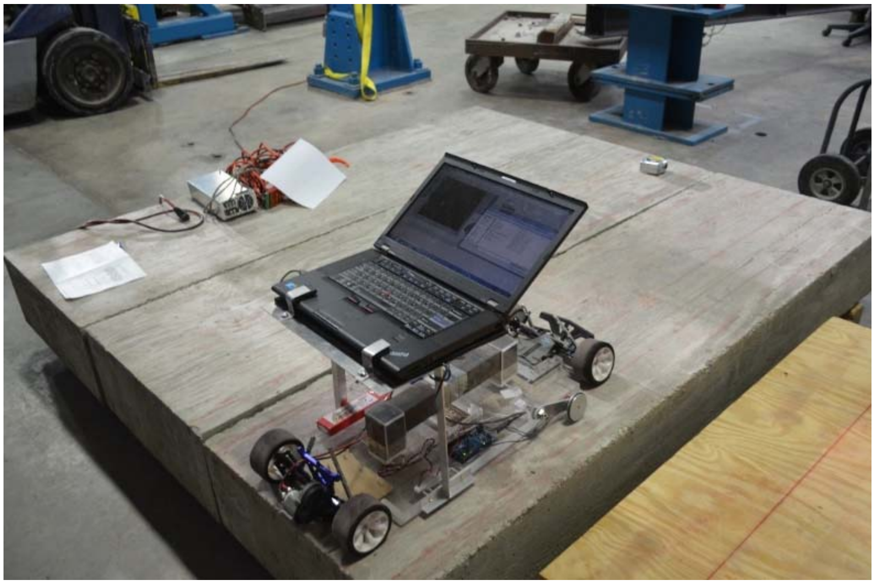

Figure 3.2: Specimen 2 Beams, S2-1, S2-2 and S2-3

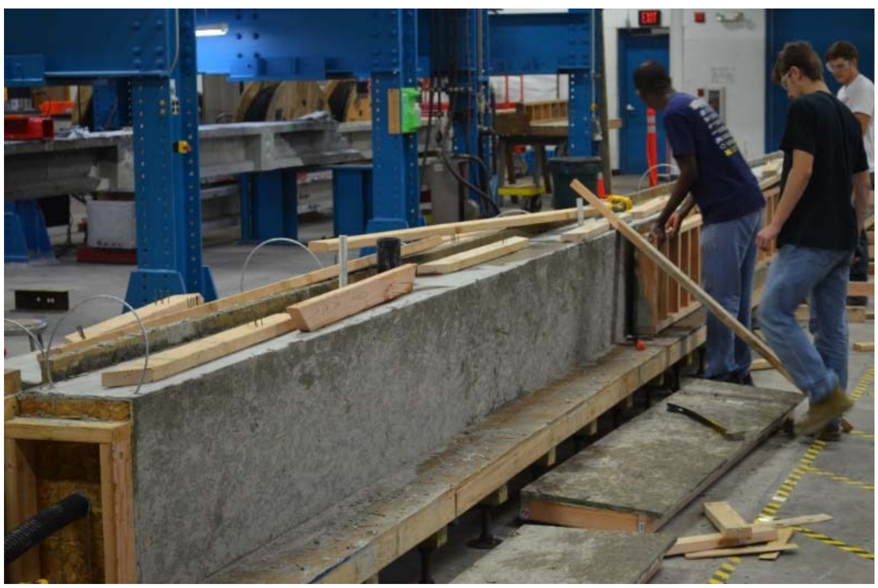

Figure 3.3: Specimen Beams, S3-1, S3-2, S3-3 and S3-4

In addition, three (3) side-by-side salvaged box beams decommissioned by Kent County Road Commission after they have been in service for 39 years were tested in the Structural Testing Laboratory at Lawrence Technological University for both nondestructive evaluation as well as residual flexural failure testing. Prior to flexural testing, the following nondestructive methods were deployed: ultrasonic assessment for delamination and void detection; electro-chemical half-cell assessment for detecting corrosive environment; impact hammer assessment of surfaces to detect variations and potential delamination; and magnetic flux leakage to determine loss of cross sectional area of reinforcement and strands. Details of all experimental procedures are presented in subsequent sections.

Field inspections were also carried out on sections of the following existing bridges in Michigan, US-131 over Muskegon River, southbound 6 miles south of Big Rapids and segments of I-96 over Canal Road in Lansing. The employed nondestructive evaluation methods were ultrasonic, magnetic flux leakage and electro-chemical half-cell assessments.

3.2. Construction of Two Samples of Specimen 1 Box Beams, S1-1 and S1-2

Two 15 feet long box beams were constructed with a cross section of 27 in x 36 in and in concept designed according to MDOT Bridge Design Guides 6.65.10A with single layer of bottom reinforcement. These laboratory beams represents box beam members in a typical reference bridge with a span length of 60 feet and a deck width of 45 feet. The bridge would allow one lane of traffic in each direction and two shoulders of 10 feet width. The laboratory beams were reduced in length from 60 feet to 15 feet while still including a center transverse diaphragm and two cells. This reduction enabled transporting the beams with the available lifts. Furthermore, due to the limited scope of this project, no deck slab was incorporated during the construction of the beams, and therefore, shear stirrups were not extended to integrate a slab system.

3.2.1 Design and Construction of Formwork.

The formwork was constructed mainly from plywood and consisted of base chairs, base-plates and side plates. The base plate was supported on base chairs at a spacing of two feet along the length of the base plate. Horizontal and vertical braces were also provided to support the side-plates and to ensure straight alignment of the edges of the box-beams.

Interior cells were constructed using plywood boxes. The cells were fixed in place by suspending them on threaded rods with end nuts outside the formwork. In the laboratory setting the final placement of the cells were well controlled. For instance, one of the cells was intentionally shifted horizontally towards one side of one box beam to create a thinner web. The intention was to evaluate the effectiveness of the phased array 3D ultrasonic tomography method to detect and quantify defects in the thinner web. Formwork was designed and constructed in the laboratory by research assistants and laboratory technical staff as shown in Figures 3.4 through 3.6.

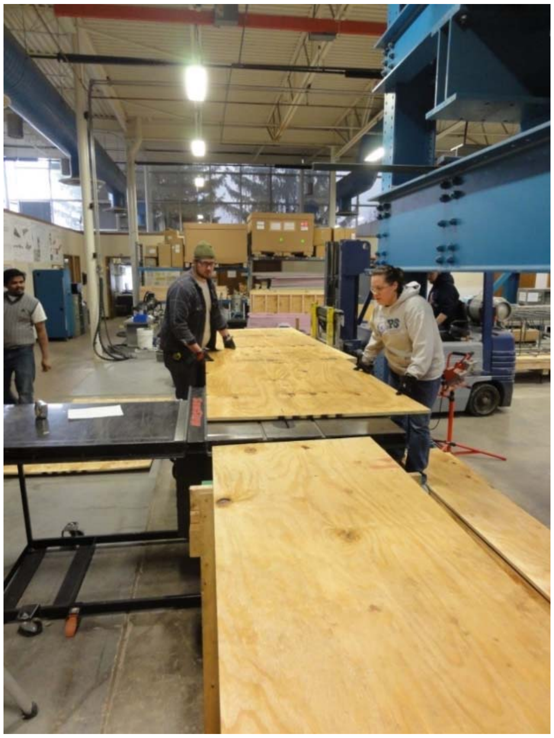

Figure 3.4: Construction of formwork.

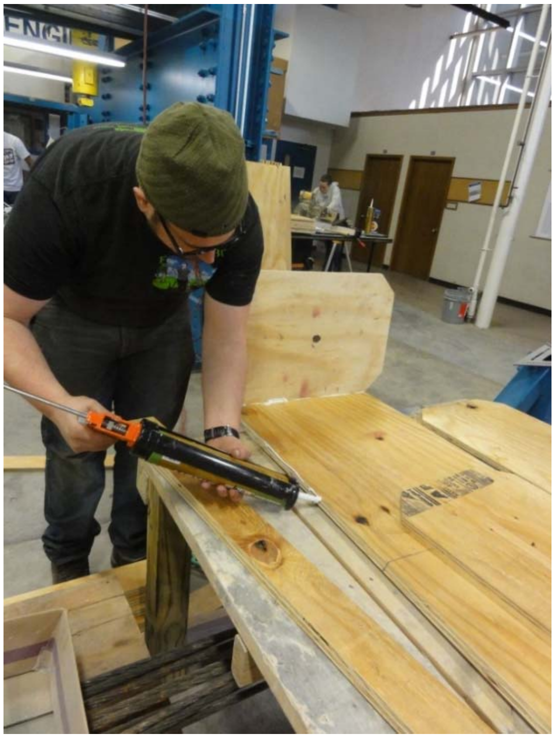

Figure 3.5: Construction of interior cells

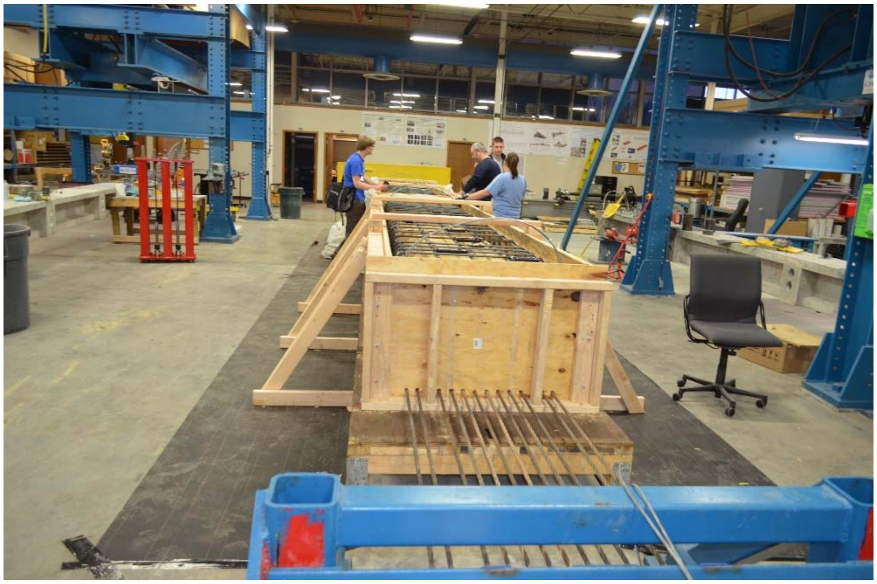

Figure 3.6: Formwork set-up

3.2.2 Reinforcement Cages

All reinforcements were cut, bent and installed in the laboratory. Each box-beam cage was made up of mild steel #4 steel stirrups at different spacing and five #4 non-prestressing bars provided as top and bottom reinforcement according to MDOT Bridge Design Guides 6.65.10A. The center of top reinforcements were located at 2.5 inches from the top surface of the beam. The mild steel, longitudinal bars and stirrups, for the box beams reinforcement were Grade 60.

In addition, there were a total of 12 prestressing steel strands located at the bottom of the beam. The steel prestressing strands were Grade 270 relaxed strands with diameter of 0.6 inch. The center of the prestressing strands were located at 2 inches from the bottom surface of the beam. A total prestressing force of 280 kips was symmetrically distributed among the bottom steel strands along the cross section of each beam as follows: 4 strands were stressed 10 kips each, another 4 were stressed 23 kips each, 2 out of the remaining 4 were stressed 30 kips each and the remaining 2 were stressed 44 kips. Details of the cross-section and longitudinal sections of the beams have been provided in Figures 3.7 and 3.8. Figures 3.9 through 3.12 depicts the preparation and installation of rebar for S1-1 and S1-2.

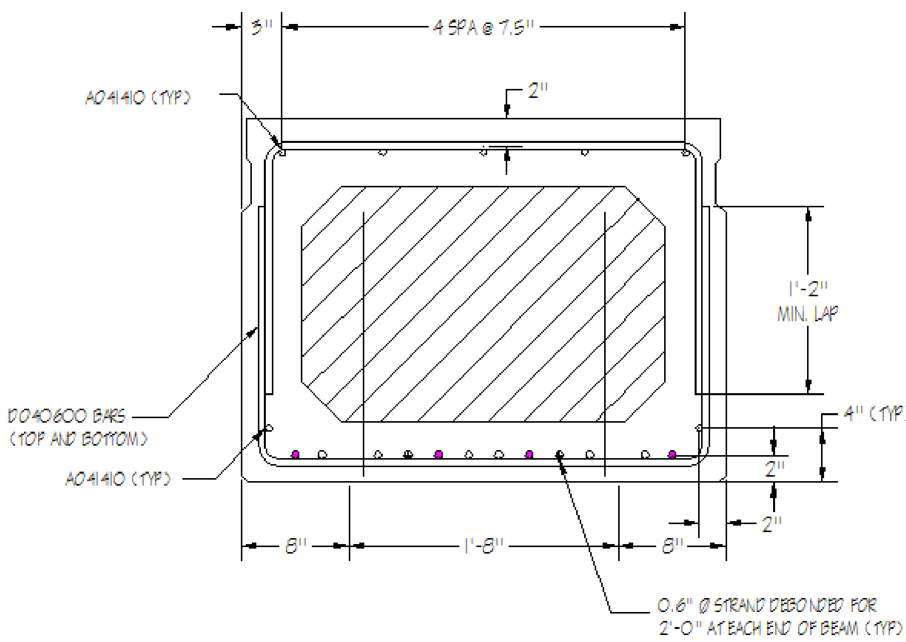

Figure 3.7: Cross-sectional details of box-beams

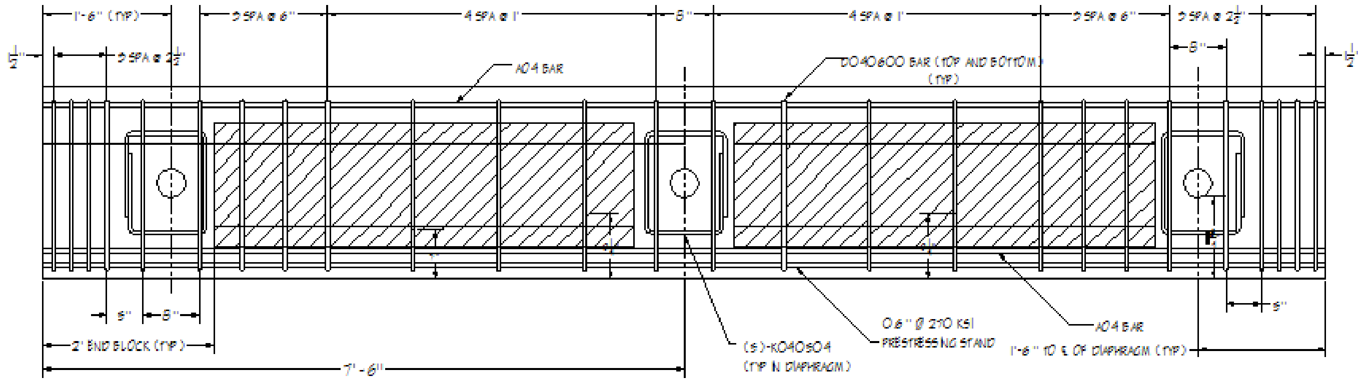

Figure 3.8: Longitudinal details of box-beams

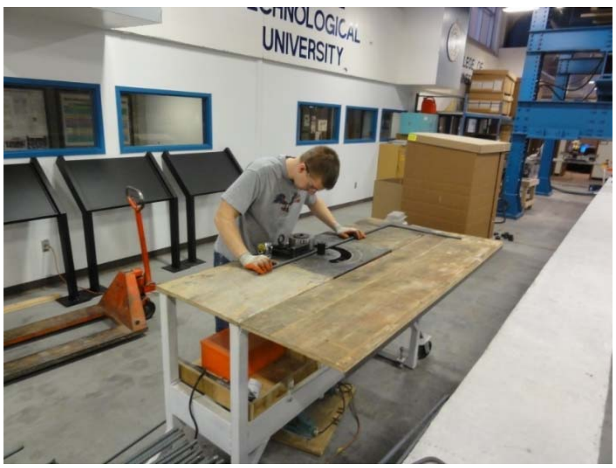

Figure 3.9: Bending stirrups

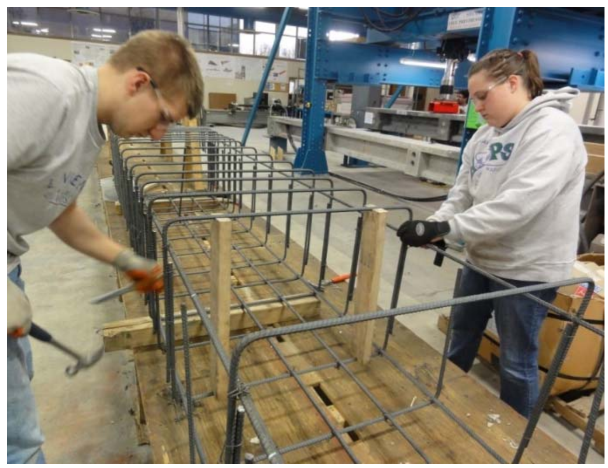

Figure 3.10: Assembling of reinforcement

Figure 3.11: Reinforcement cages for box-beam

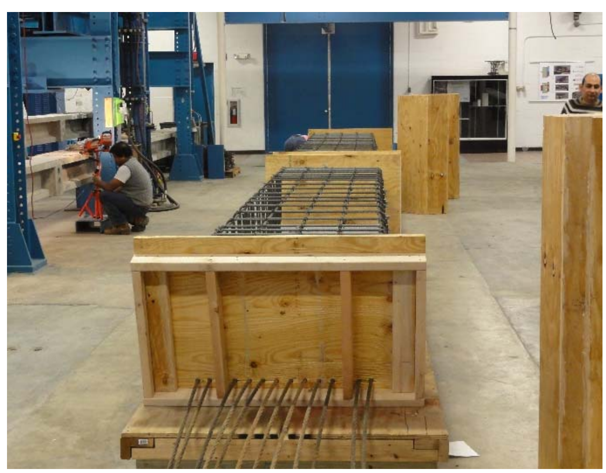

Figure 3.12: Installing edge & side Panels

3.2.3 Simulation of Defects

Defects of voids were simulated along the length of reinforcement to depict voids created around reinforcement as a result of the corrosion process, see Figures 3.13 through 3.16. Furthermore, two additional types of defects were used; three (3) simulated honeycombs and heavy grease around several of the prestressing strands. The goal of these activities were to determine if these defects could be detected using the phased array ultrasonic 3D tomography. The defect types and their locations were documented as shown in Figures 3.17 through 3.19.

Fig. 3.13: Plastic defects around reinforcement

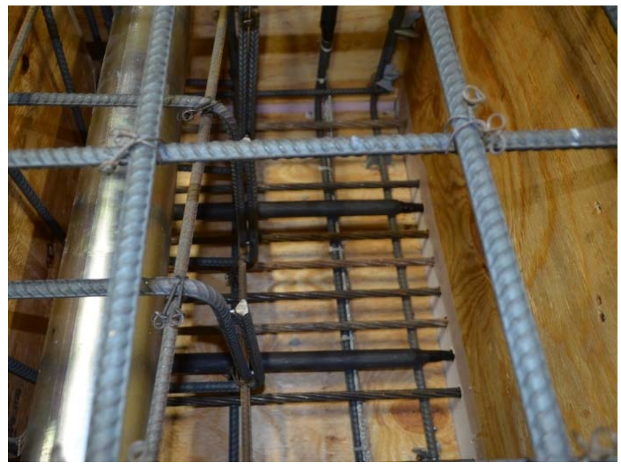

Fig. 3.14: Plastic defects around bottom strand

Fig. 3.15: Honeycomb at the top of box beam

Fig. 3.16: Plastic tubes for debonding

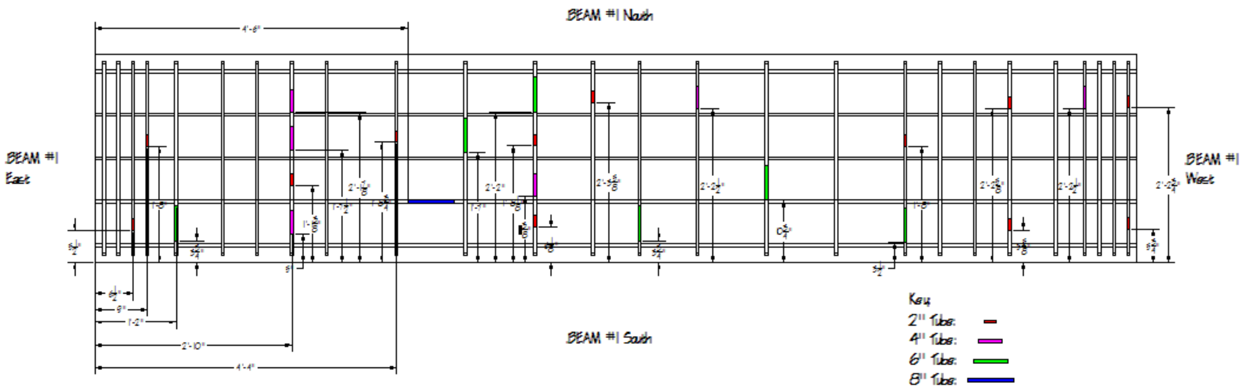

Figure 3.17: Top plan of box beam showing locations and defect length around Top reinforcement

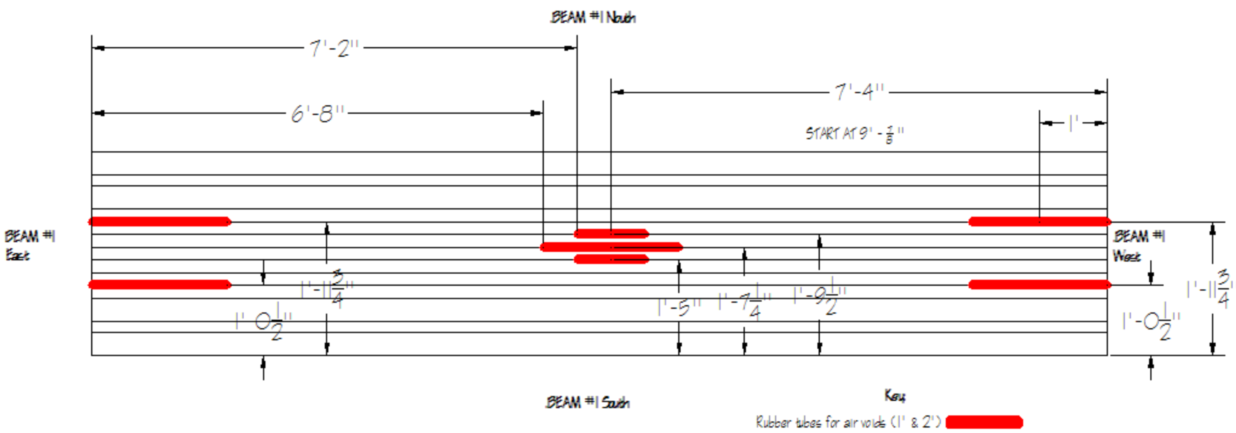

Figure 3.18: Bottom Plan of Box Beam 1 showing locations of defects around strands

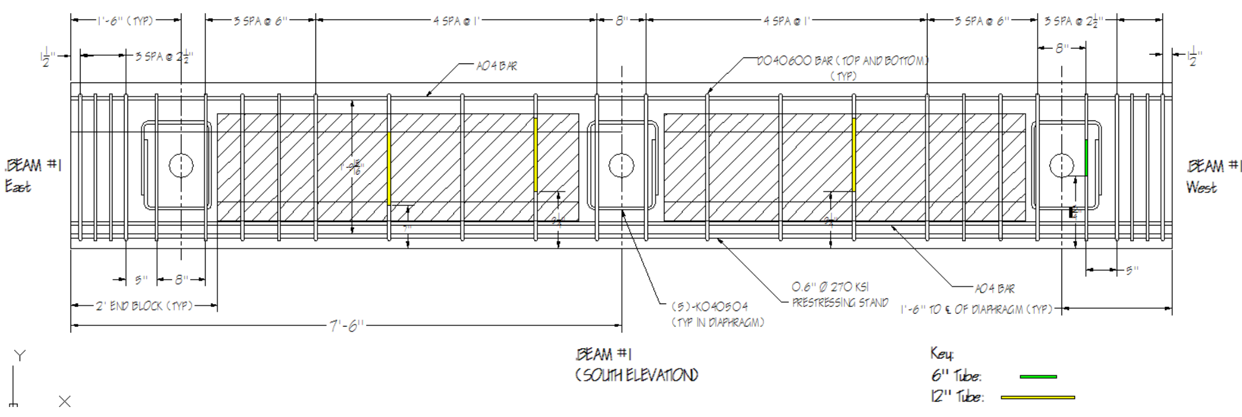

Figure 3.19: South Elevation of Box Beam 1 showing locations of defects around strands

3.2.4 Prestressing Steel Strands

End plates for the prestressing bed were redesigned to suit the proposed beam size and to fit for the strands spacing as shown in Figure 3.20

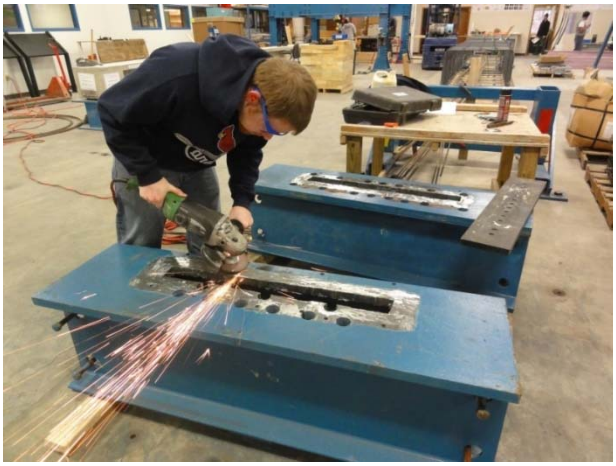

Figure 3.20: End plates for prestressing bed.

Figure 3.21: Prestressing steel strands

When construction of the steel cages and formwork were completed, the steel cages were placed inside the formork. Plastic chairs with effective height of 1.5 in were attached to the underside of the cages to provide the bottom cover. In addition, 1.25 in chairs were also attached to either side of the cages to create the side concrete cover. Bulkheads were mounted at the two extreme ends of the two beams. Conventional steel chucks were used as anchorage systems for the steel strands and attached at both the live and dead-ends of the steel strands. Figure 3.21 depicts the application of prestressing forces to the strands.

3.2.5 Concrete Placement and Preparation of Cylinders.

Six (6) cubic yards of concrete with compressive strength of 7000 psi ordered from MCCOIG Materials was used for the casting of the two (2) box beams and preparation of 24 concrete cylinders for compressive strength testing as shown in Figures 3.22 and 3.23. Two slump tests were conducted prior to casting of the box-beams and immediately after in accordance with ASTM C143/C143-05 to check the workability of the concrete. Two electrical vibrators were used for consolidation as well as mechanical rods around the diaphragm locations and the end-block of the beams where the steel reinforcements were closely spaced.

Figure 3.22: Casting of Box Beams, S1-1 and S1-2

Fig. 3.23: Slump Test / Cylinders Preparation

3.2.6 Curing Box Beams and Releasing of Steel Strands

The beams were cured under wet burlaps layered with plastic sheets to limit moisture loss and surface cracking. Water was applied to the top beam surfaces for 7 days. Steel strands were released after 4 days of curing by cutting them from the bulkheads in order to transfer the compressive stresses to the concrete after it had gained adequate strength.

Figure 3.24: Curing Beams

Figure 3.25: Releasing of steel strands.

3.2.7 Compressive Strength of Box Beams

The average 28 day compressive strength of the cylinders was 7,694 psi. The development of average compressive strength with age and the summative data are shown in Table 1. The compressive strength was determined according to ASTM C39 - 05, Standard Test Method for Compressive Strength of Cylindrical Concrete Specimens. Figures 3.26 and 3.27 shows compressive strength testing for 4 days and 7 days respectively, the prestressing force was transferred at the 4 days compressive strength.

Table 3.1: Compressive Strength Development using 6 inch by 12 inch Cylinders

Identification Number	Max. Load (Pound-force)	Compressive Strength (psi)	Age of specimen (days)
C1	106,990	3,784	4
C2	118,320	4,185	4
C3	112,070	3,964	4
C4	142,470	5,039	7
C5	139,050	4,918	7
C6	147,400	5,213	7
C7	182,260	6,446	14
C8	201,780	7,137	14
C9	179,650	6,354	14
C10	207,050	7,323	28
C11	218,790	7,738	28
C12	226,750	8,020	28

Fig. 3.26: Four (4) Days at Transfer

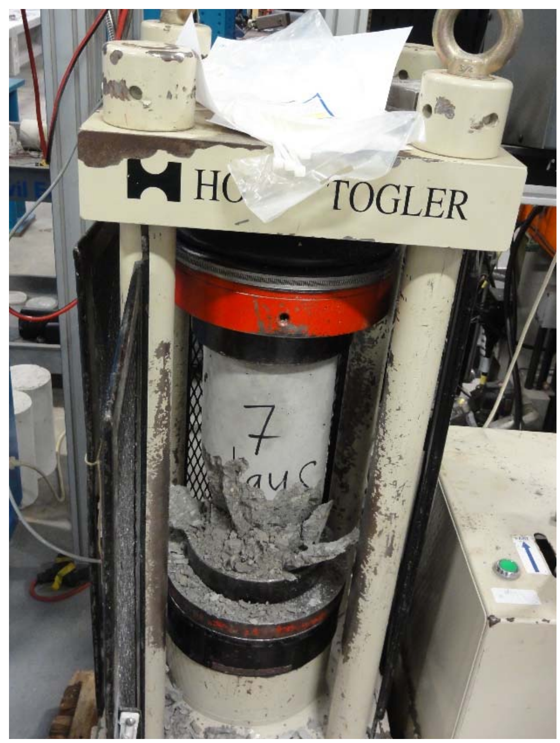

Fig. 3.27: 7 Days Compressive Strength

3.2.8 Ultrasonic Assessment of S1-1 and S1-2.

Testing was done by scanning the entire geometry of the box beams to ascertain how correctly the ultrasonic assessment predicts the thicknesses of the various components of the box beams. This was used as a reference during scanning of strands, for instance to check on the location of strand from the concrete surface a reference was made to the thickness of the bottom flange.

The following testing protocol was used for S1-1 and S1-2.

(i) Complete scan of all four longitudinal surfaces of each beam with varied frequencies of 30, 40, 50, 60, 70, 80, 90 and 100 kHz to examine how the different thicknesses of the various components of the beam were predicted with the above frequencies.

(ii) Localized scan on defects: plastic tubes (denoting voids and debonding) and grease with varied frequencies of 30, 40, 50, 60, 70, 80, 90 & 100 kHz to simulate assessment of voids which usually occur around corroded strands and reinforcement as a result of corrosion.

(iii) Localized scan on defects: honey combs with frequencies of 30, 40, 50, 70, 80, 90 & 100 kHz to simulate deterioration in concrete structures such as cracks and delamination which usually occurs as a result of corrosion of strands and reinforcement.

(iv) Localized scan on reinforcement and strands without defect, with frequencies of 30, 40, 50, 60, 70, 80, 90 & 100kHz were compared with localized scan on plastic defects to check on the differences of the various scans.

(v) Localized scan on solid concrete sections without reinforcement, strand or any defect, with frequencies of 30, 40, 50, 60, 70, 80, 90 & 100 kHz

Figures 3.28 through 3.30 show ultrasonic assessment from various locations along box beams S1-1 and S1-2. Detailed analysis of the test results have been presented in sections 4.1 and 4.2.

Figure 3.28: Scanning on the side of S1-1

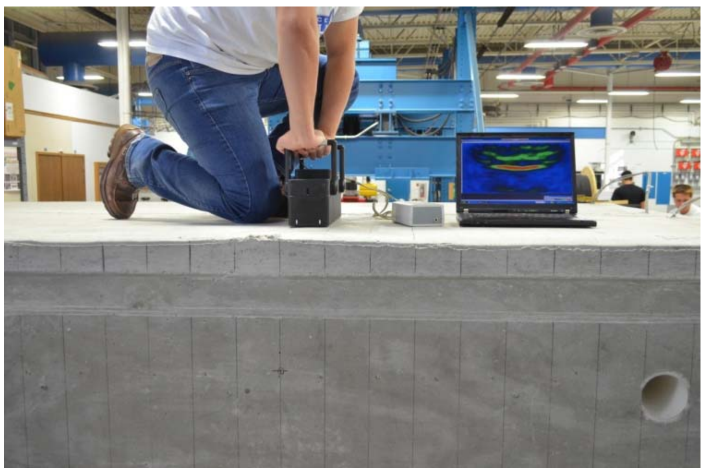

Figure 3.29: Scanning on top of S1-2

Figure 3.30: Scanning on the bottom of S1-2

3.3 Construction and Testing of Three Specimen 2 Beams

3.3.1 Construction of Specimen 2 Beams

3.3.1.1 Formwork and Preparation of Reinforcement/Strands

Formwork was designed and constructed in house in the laboratory by research assistants and laboratory technical staff. Three sets of formwork were constructed to simulate three different samples of Specimen 2 as shown in Figure 3.31. Reinforcement were cut and grinded to the required percentage losses of cross-sectional areas as shown in Figure 3.32. The percentage losses considered were 5, 10, 15, 20 and 30 with varying lengths of grinding along the reinforcement. Two lengths of grinding configurations considered were 1inch-1inch-1inch and 5inches-2inches-5inches as shown in Figures 3.33 and 3.34. Wires along 0.6 diameter strands were also cut varying from one wire cut to four wires cut with varying cutting lengths of 0.25 inch to 1 inch and were covered with dual-wall polyolefin plus duct tape as shown in Figure 3.36.

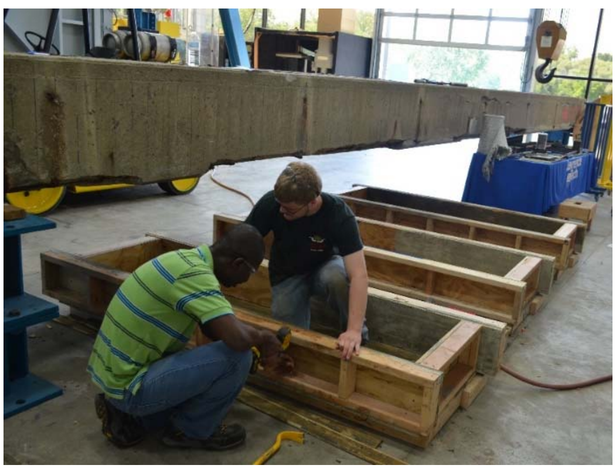

Fig. 3.31: Constructing formwork

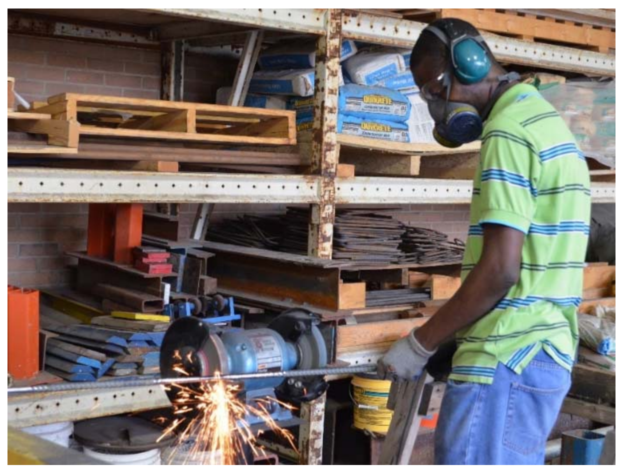

Fig. 3.32: Cross-sectional area loss on reinforcement

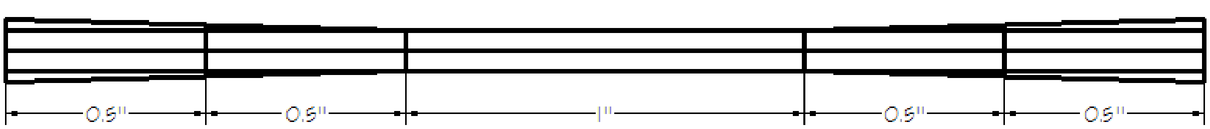

Fig. 3.33: Grinding configuration of 1(0.5+0.5)inch-1inch-1(0.5+0.5)inch for different percentage losses for reinforcementbar

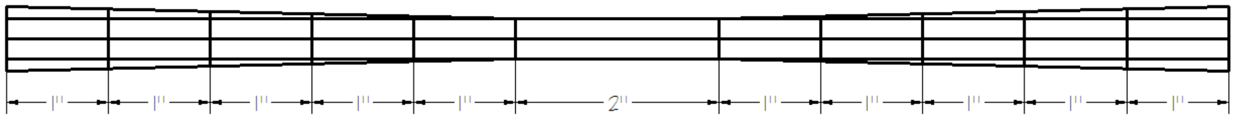

Figure 3.34: Grinding configuration of 5(1+1+1+1+1) inches-2 inches-5(1+1+1+1+1) inches for different percentage losses for reinforcement

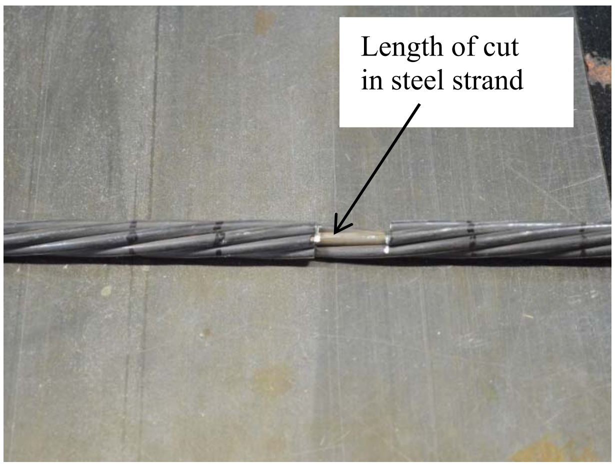

Figure 3.35: 0.6" Strand length of wire cut

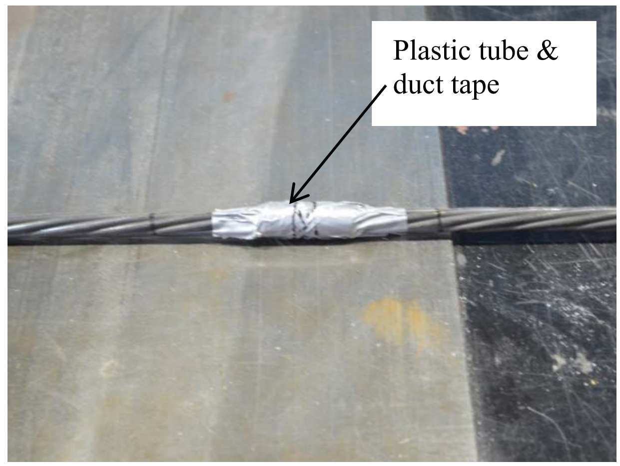

Figure 3.36: Wire cut covered with dual wall Polyolefin tube and duct tape

3.3.1.2 Preparing the cages

Reinforcemnet and strands were tied with documented defect locations as shown in Figures 3.37 through 3.39. Three sets of cages were formed, one for single layer of top and bottom reinforcement with defects in both top and bottom reinforcement, a second with double bottom layer of reinforcement with defects in both top reinforcement as well as second layer of reinforcemnt from the bottom. A third was formed for single layer of top strands with double layer of bottom strands with defects in the top strands and the second layer of strands from the bottom. The reinforcement grinded to simulate cross-sectional area losses were #5 steel of Grade 60 with #3 stirrups of Grade 60. The longitudinal prestressing strands with wire cuts to simulate cross-sectional area losses were 0.6 in, low-relaxation seven-wire steel strands of Grade 270.

Figure 3.37: Cages of reinforcement and strands

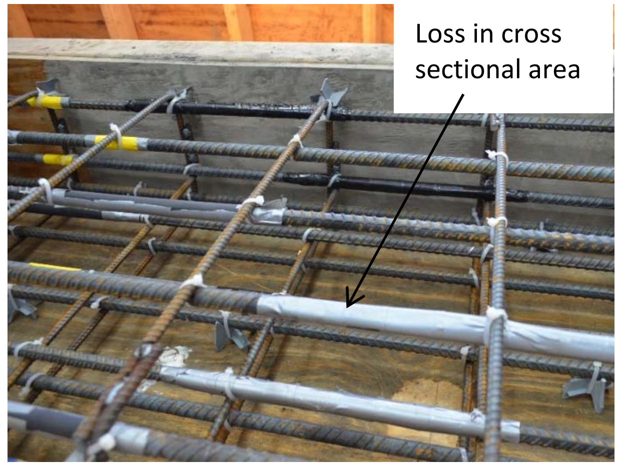

Figure 3.38: Cross-sectional Area loss

Figure 3.39: Strands showing loss of wires covered with Dual wall polyolefin tube and duct tape

3.3.1.3 Placing of Concrete and Preparation of Concrete Cylinders

Two cubic yards of concrete with compressive strength of 7000 psi ordered from MCCOIG Materials was used for the casting of three (3) Specimen 2 beams and preparation of cylinders for compressive strength testing as shown in Figures 3.40-43.

Fig. 3.40: Placing of concrete

Fig. 3.41: Leveling top of specimen 2 beams

Figure 3.42: Checking for slump

Figure 3.43: Preparation of concrete cylinders

3.3.2 Ultrasonic Assessment of S2-1, S2-2 and S2-3.

Ultrasonic testing of Specimen 2 beams was undertaken using the following testing protocol.

(i) Complete scan of top and bottom surfaces of each of S1-1, S2-2 and S2-3 with varied frequencies of 30, 40, 50, 60, 70, 80, 90 and 100 kHz to examine how the different cross-sectional area losses due to grinding of reinforcement and cutting of wires of strands were detected with the above frequencies.

(ii) Localized scans on defect locations with varied frequencies of 30, 40, 50, 60, 70, 80, 90 & 100 kHz

(iii) Localized scan on reinforcement and strands without defect, with frequencies of 30, 40, 50, 60, 70, 80, 90 & 100 kHz.

Details of reinforcement configurations for S2-1, S2-2 and S2-3 with documented locations of these simulated defects are shown in Figures 3.44 through 3.52. Figure 3.53 shows ultrasonic assessment set-up for S2-1. Figures 3.54 and 3.55 show typical scan on reinforcement with defect as well as scan on reinforcement without defect.

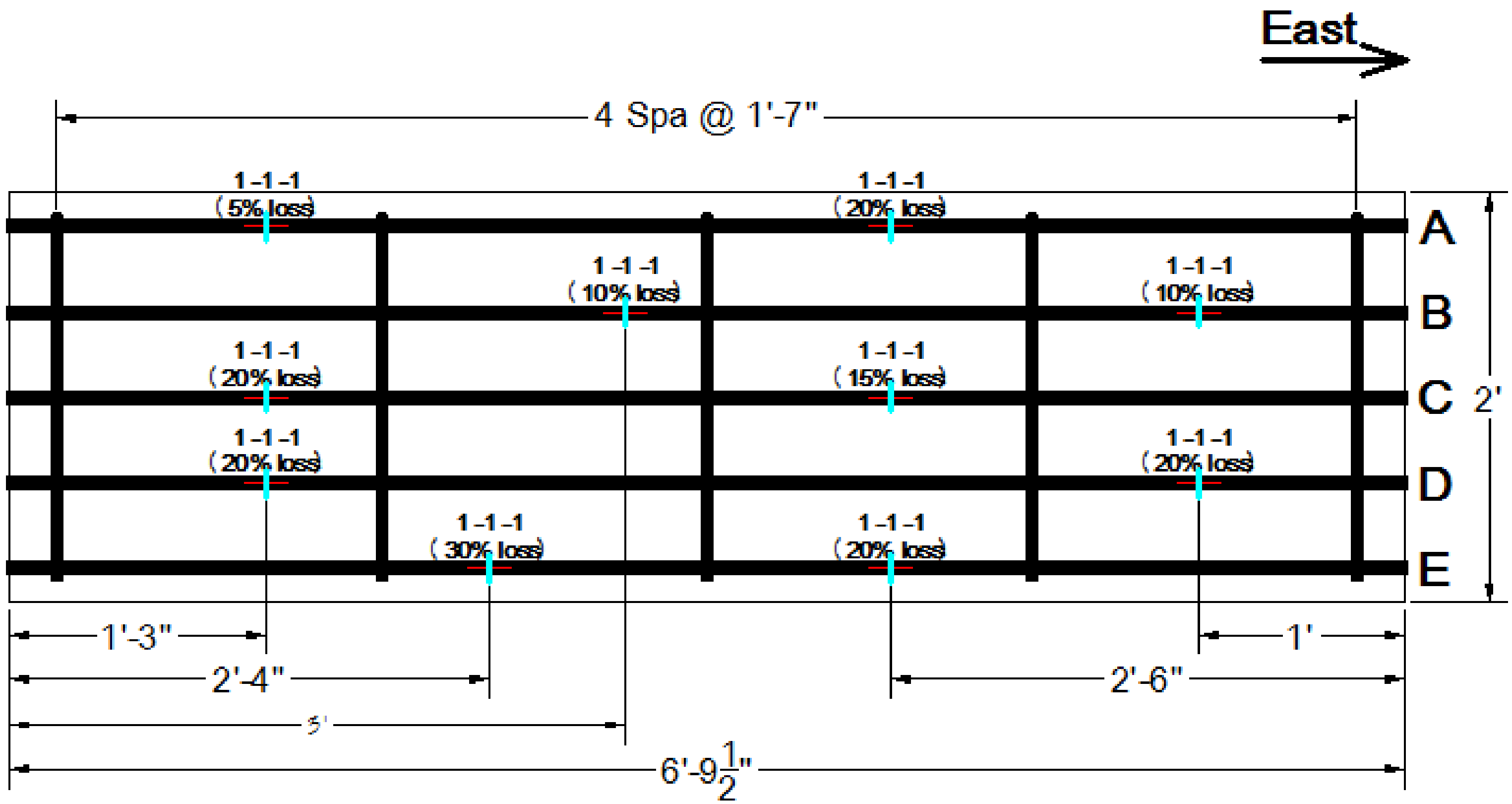

Figure 3.44: Top Reinforcement Arrangement and Percentage Losses for S2-1 with Total Length of 3 inches Cross-sectional Area Loss

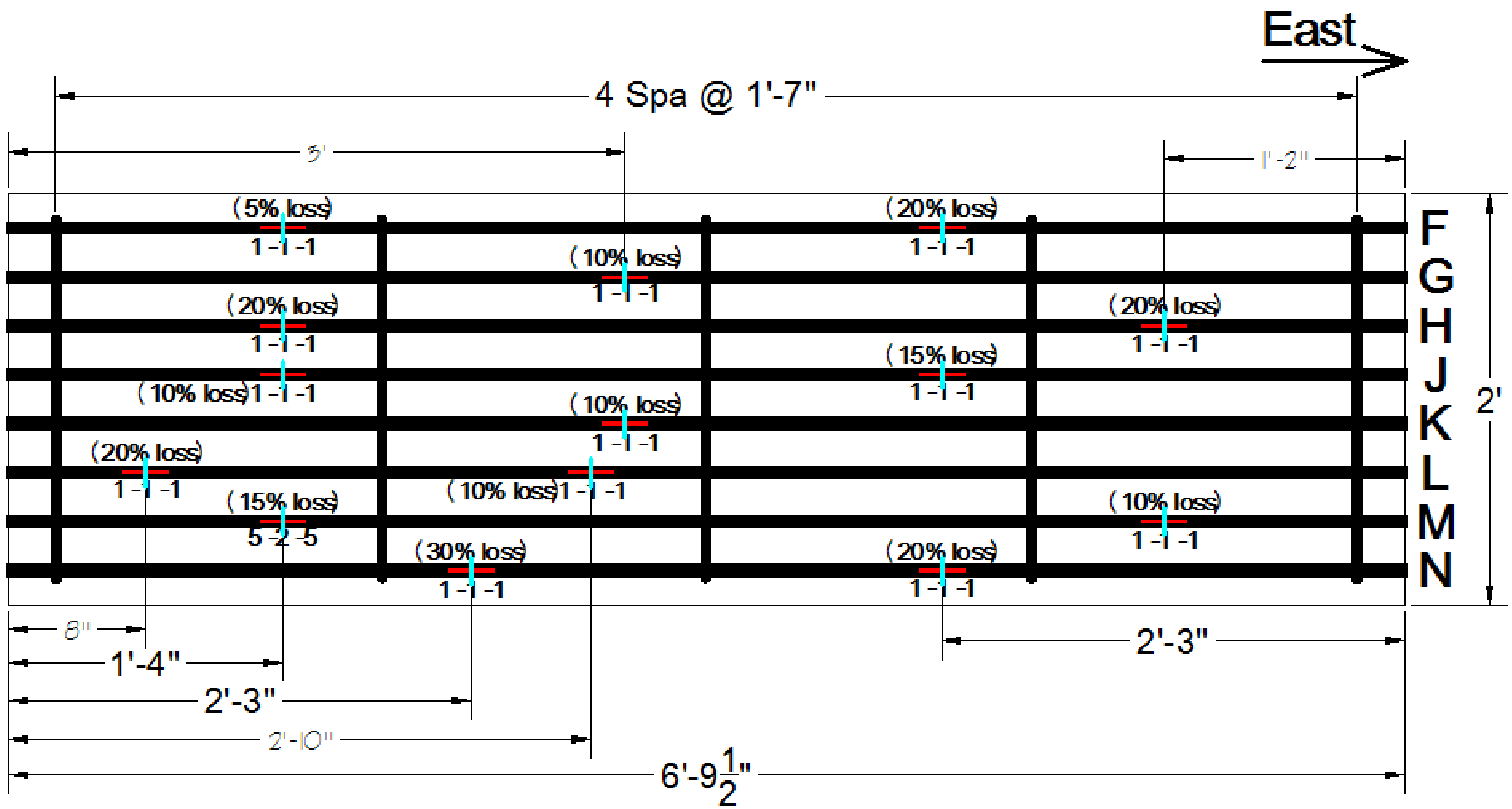

Figure 3.45: Bottom Reinforcement Arrangement and Percentage Losses for S2-1 with Total length of 3 inches Cross-sectional Area Loss

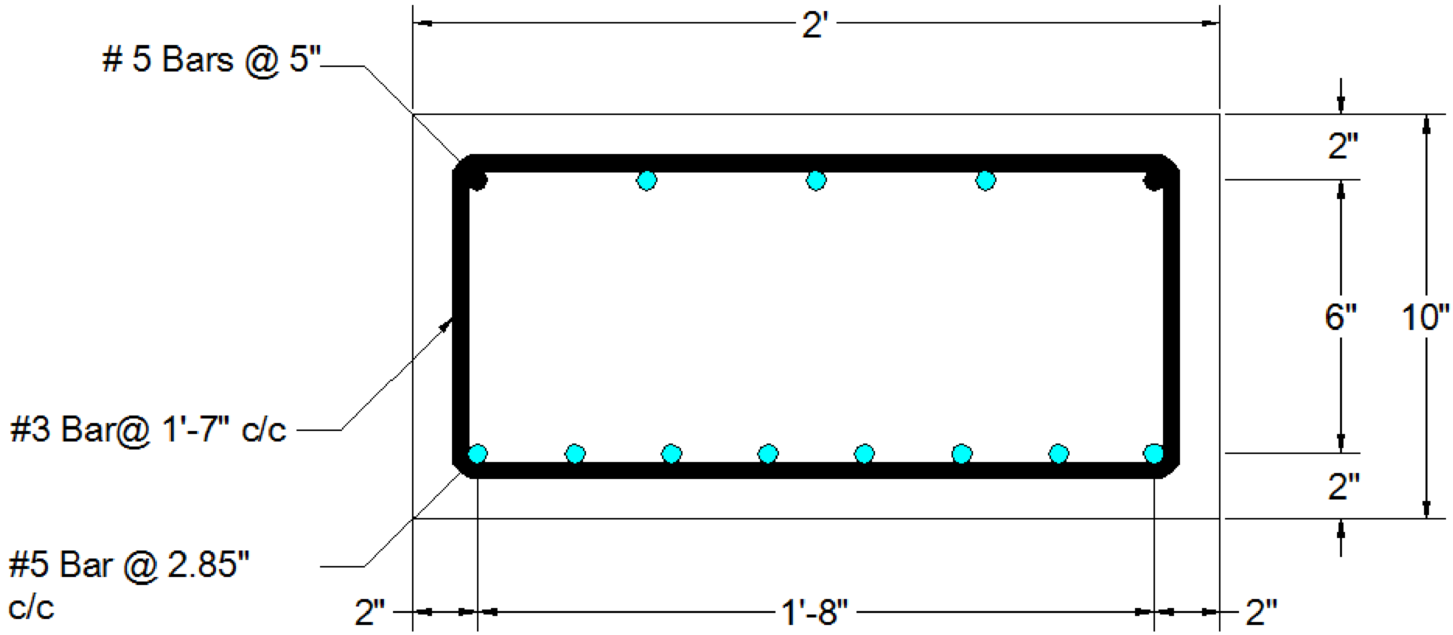

Figure 3.46: Cross-sectional Area of S2-1 showing Single Bottom Reinforcement

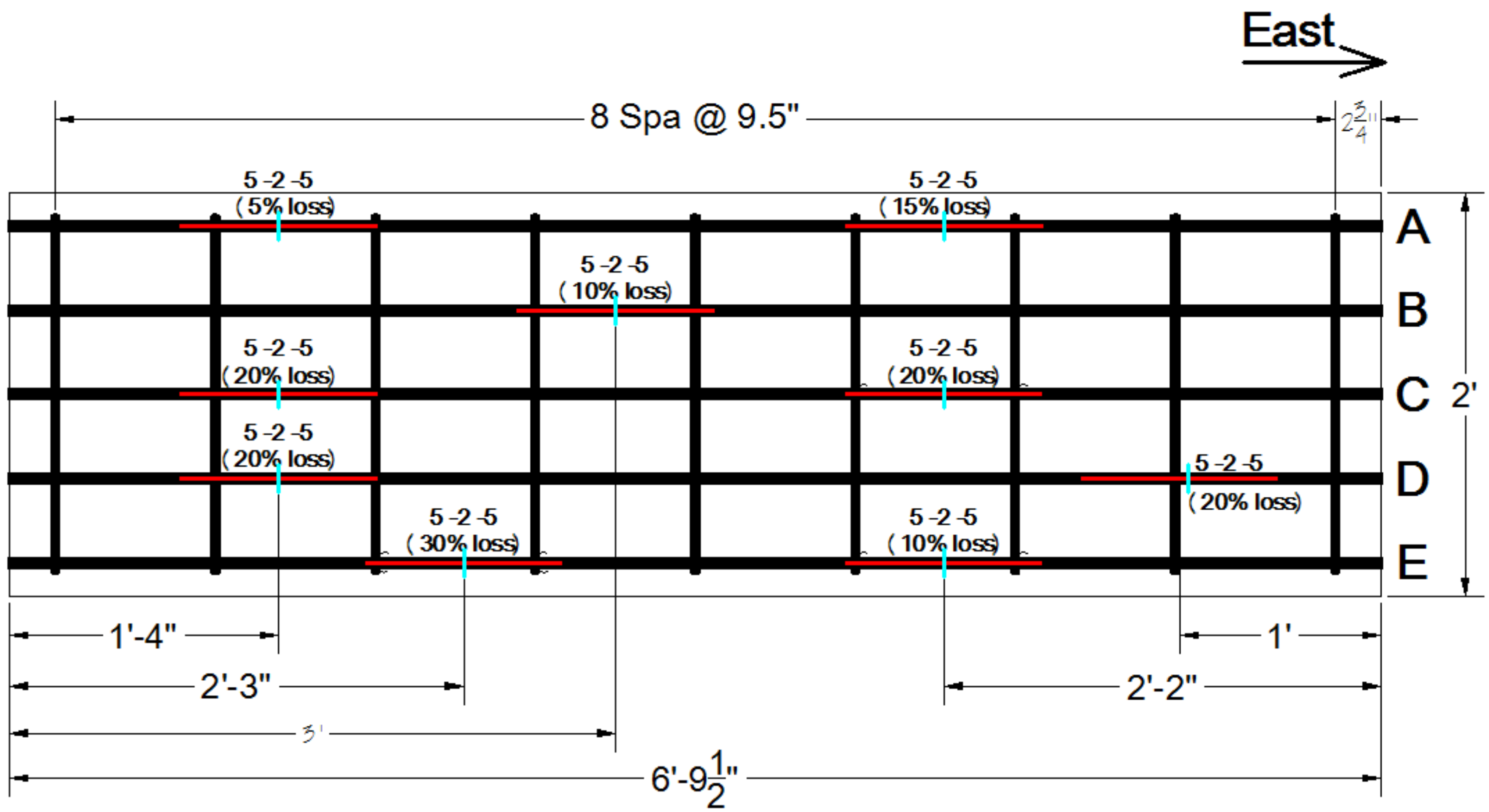

Figure 3.47: Top Reinforcement Arrangement and Percentage Losses for S2-2 with Total Length of 12 inches Cross-sectional Area Loss

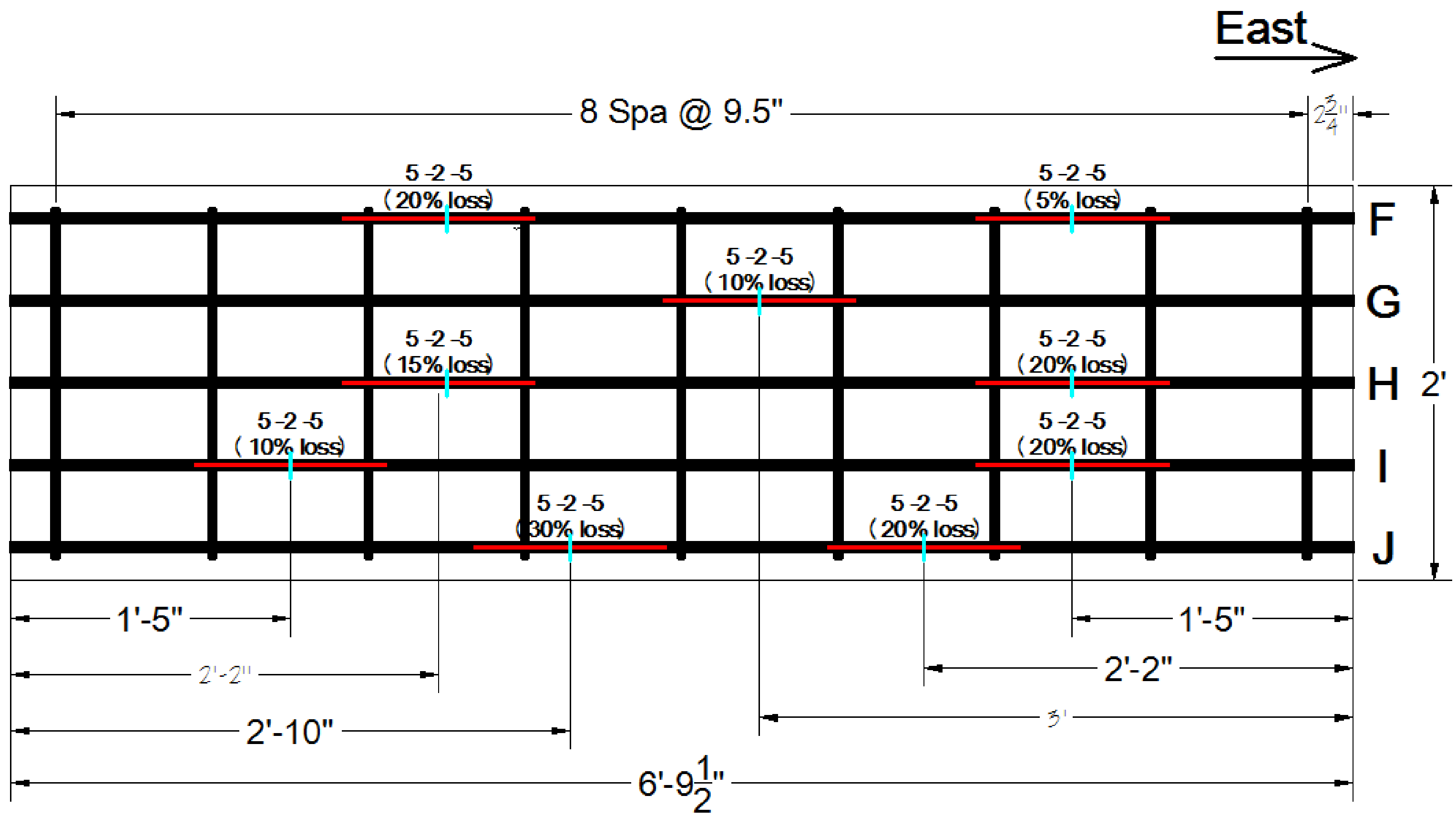

Figure 3.48: Bottom Reinforcement Arrangement and Percentage Losses for S2-2 with Total Length of 12 inches Cross-sectional Area Loss

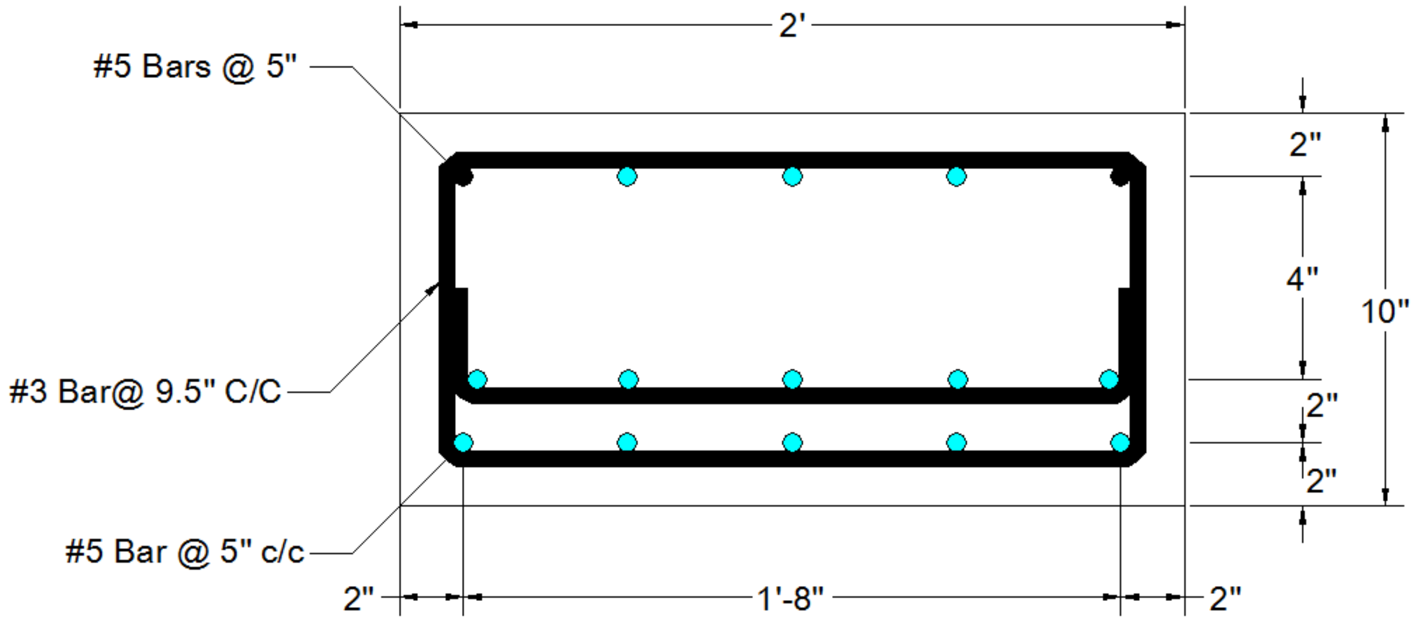

Figure 3.49: Cross-sectional Area of S2-2 showing Double Bottom Reinforcement

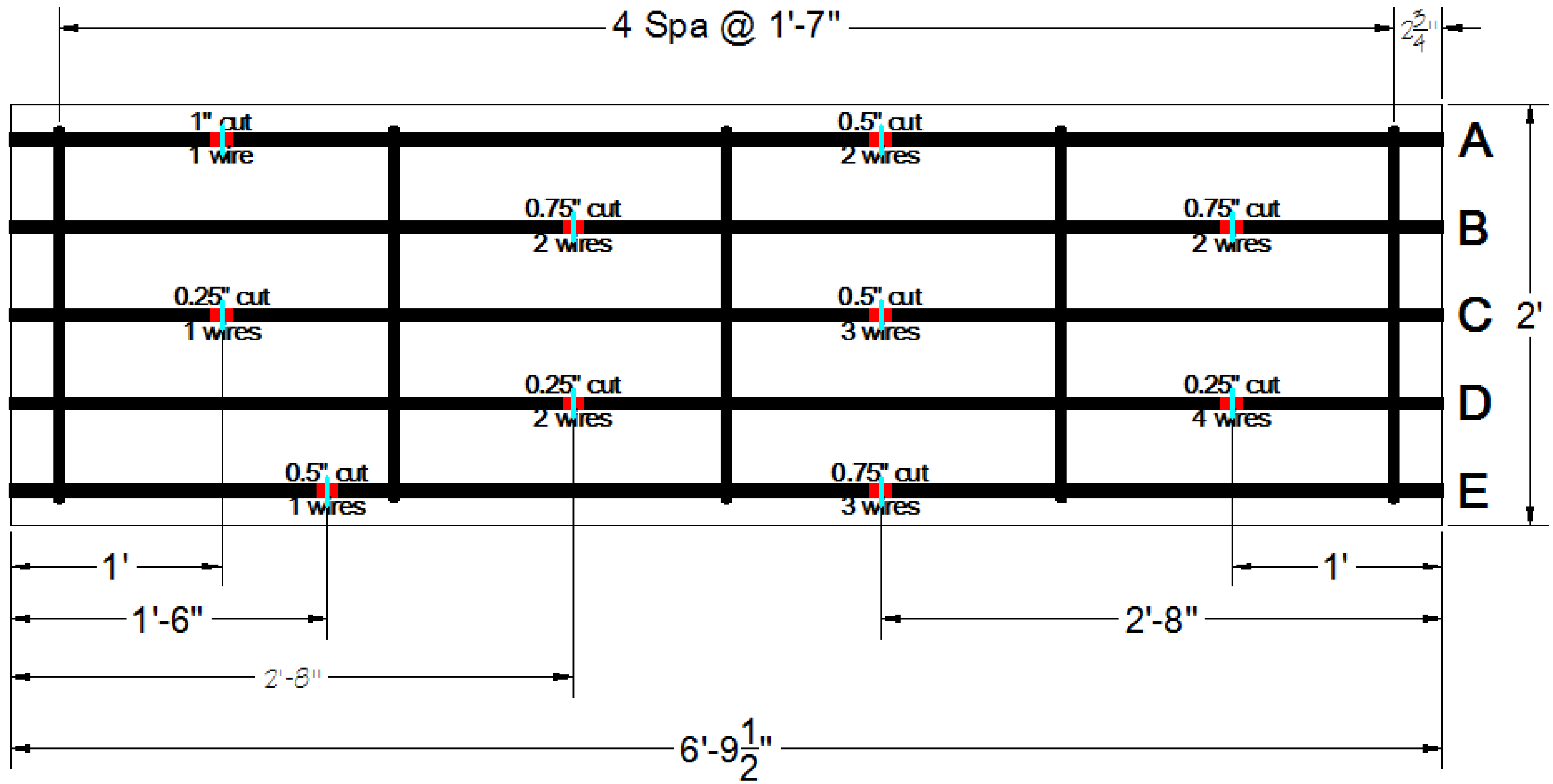

Figure 3.50: Top Strand Arrangement, Length and Number of Wire cuts for S2-3

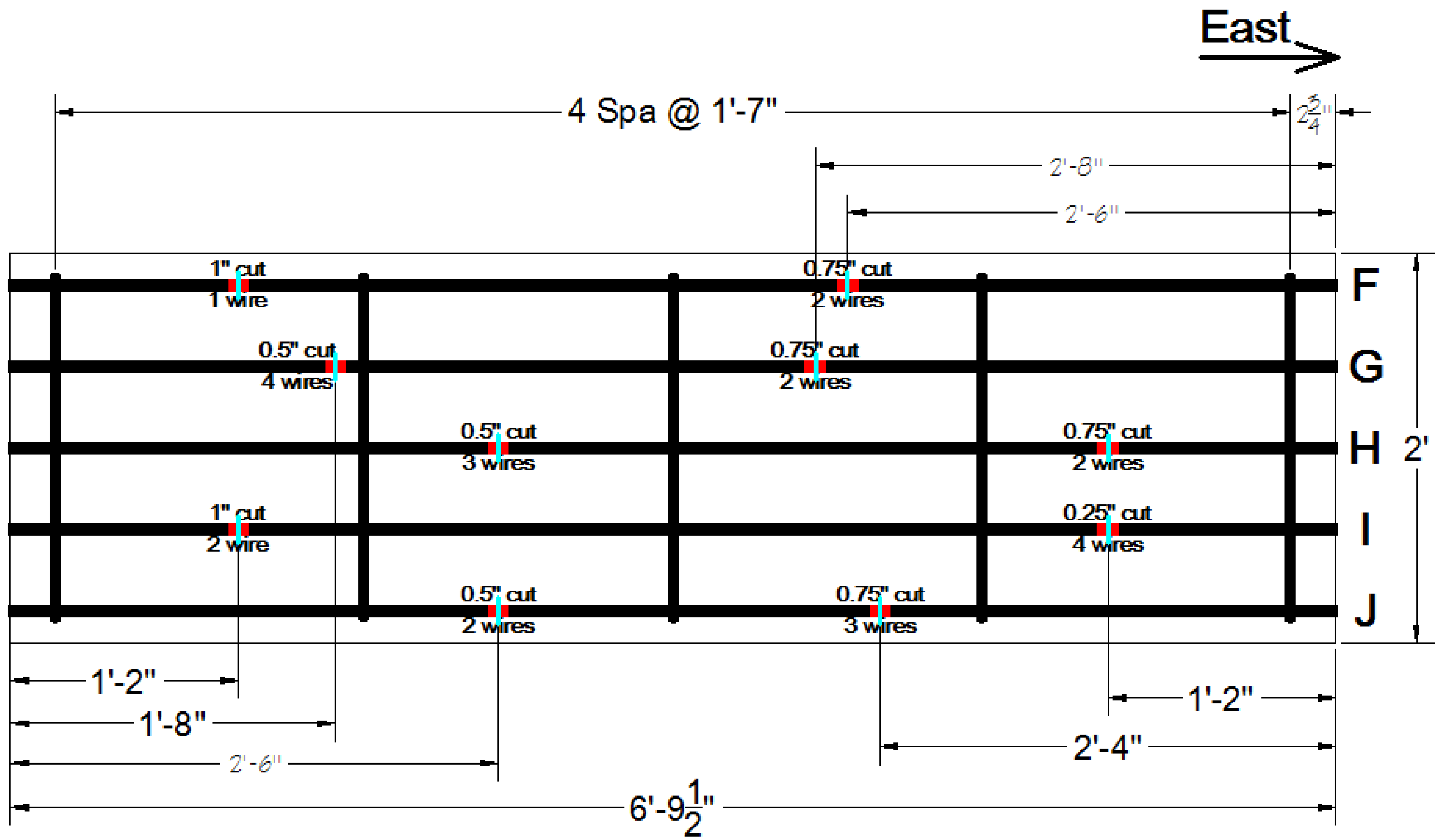

Figure 3.51: Bottom Strand Arrangement, Length and Number of Wire cuts for S2-3

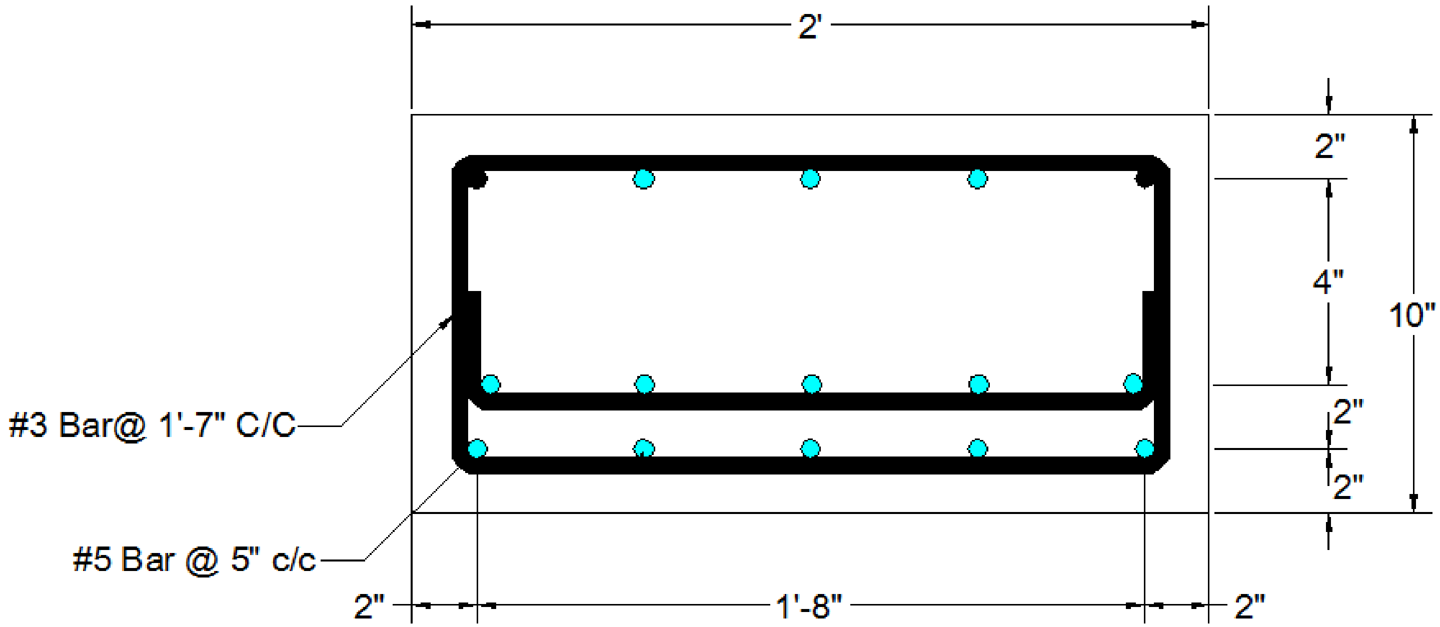

Figure 3.52: Cross-sectional Area of S2-3 showing Double Bottom Strands

Figure 3.53: Ultrasonic assessment set-up for S2-1.

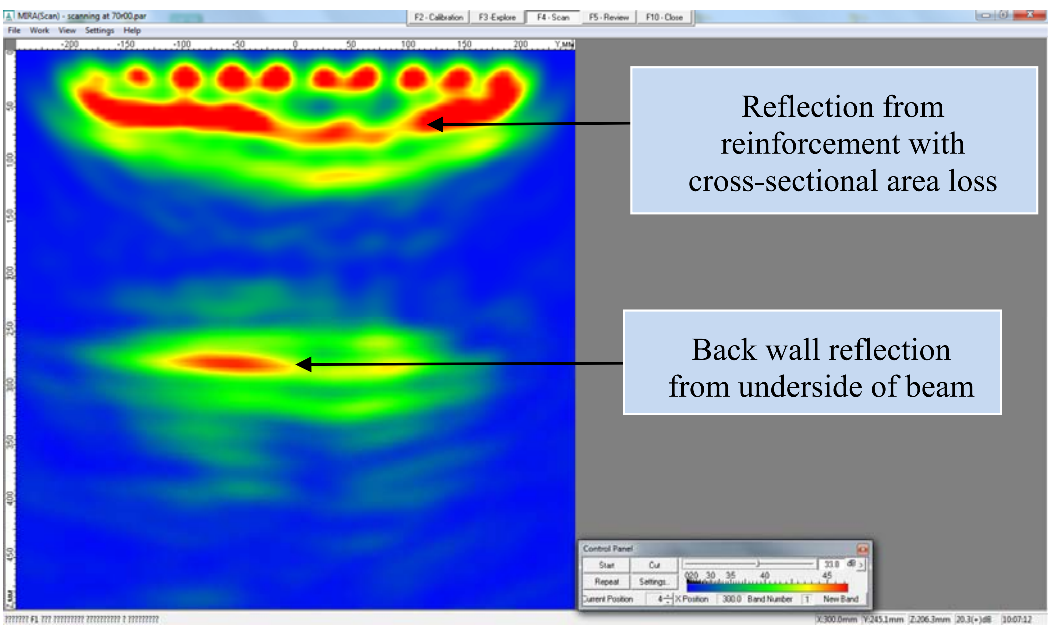

Figure 3.54: Scan on Reinforcement with defect at frequency of 70 kHz with dB of 33.8

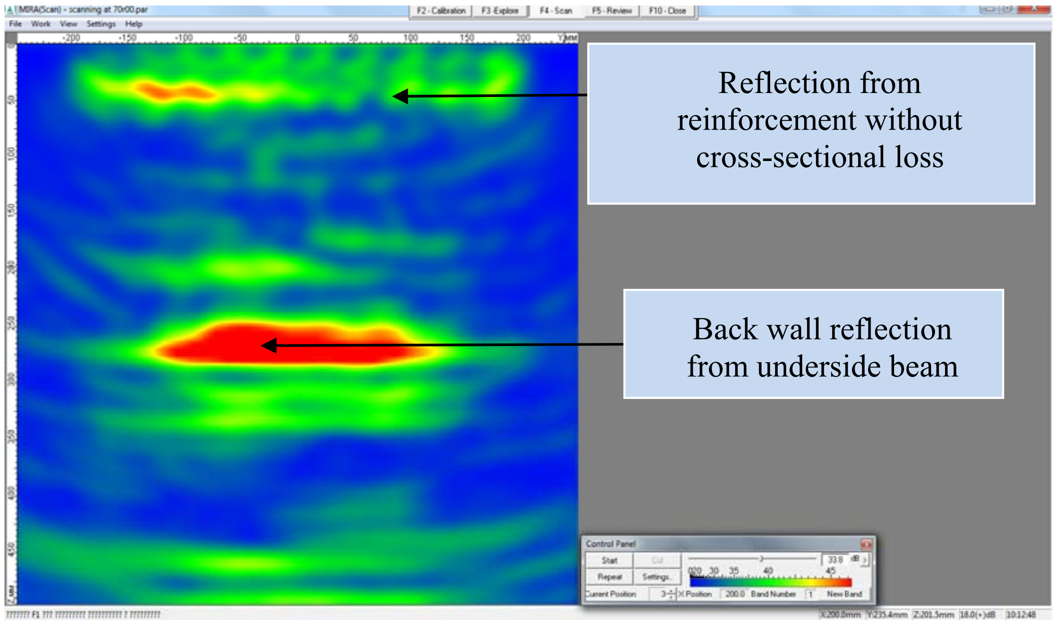

Figure 3.55: Scan on reinforcement without defect at frequency of 70 kHz with dB of 33.8

3.3.3 Calibration of Magnetic Flux Leakage (MFL) Mobile Scanner

Calibration of the MFL Mobile scanner was done, using undamaged reinforcement with 10%, 20% and 30% loss of cross-sectional area for reinforcement #4 - #9. Two timber formworks of size 48 inches x18 inches x 11inches were constructed with three (3) 2 inches holes punched on two opposite sides of the shorter faces to calibrate the influence of the magnetic system on the reinforcement at increasing depths away from the magnetic influence as shown in Figure 3.56. The first formwork had holes at increments of 2.5 inches, while the second had holes at depths of 1.5 inches, 3 inches, and 6 inches. A baseline reading of 2.935 volts from the middle Hall-effect sensor, M3, was taken by running the scanner over the formwork with no reinforcement present. Undamaged reinforcement #4 through #9 each were scanned ten (10) times at each depth increments. The voltage reading from the middle hall-effect sensor, M3, was averaged for each run and then all ten runs were averaged together.

The process was repeated for reinforcement #4 - #9 with the center foot of the reinforcement gradually milled to a 10%, 20% and 30% loss in cross-section area. The max voltage reading, which indicates the peak voltage in the affected area, from the middle hall-effect sensor, M3, was averaged for each run and then all ten runs were averaged together.

Figure 3.57 shows the trend line of the baseline adjusted average peak voltage for each depth. The graph in Figure 3.57 shows the trend line for each depth up to three inches. Figure 3.58 shows a scan of reinforcement #7 at the 1.5 inch depth. There is an increase in voltage as the MFL mobile scanner passes over the affected area. This is due to more magnetic flux reaching the Hall-effect sensor array than would be the case if the reinforcement did not have cross-sectional loss. Figure 3.59 shows magnetic flux voltage change of #7 reinforcement at 1.5 inches depth with cross-sectional area loss of 20%.

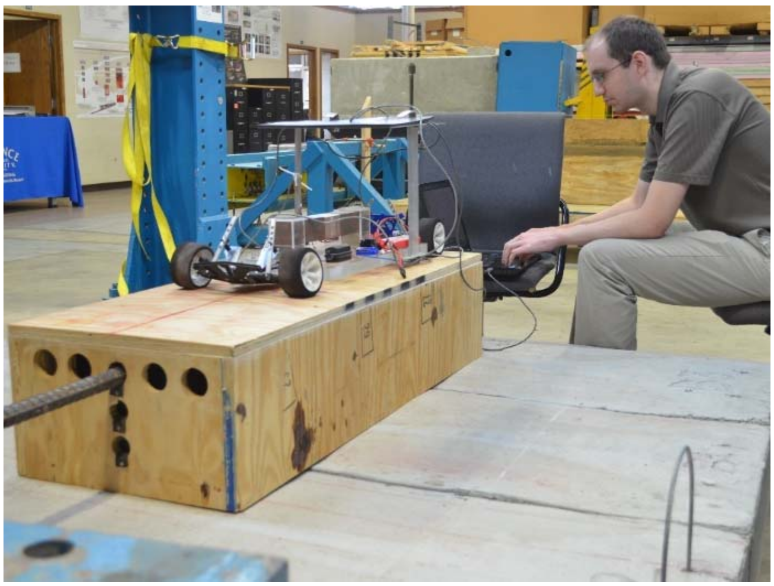

Figure 3.56: MFL Mobile Scanner Calibration Setup

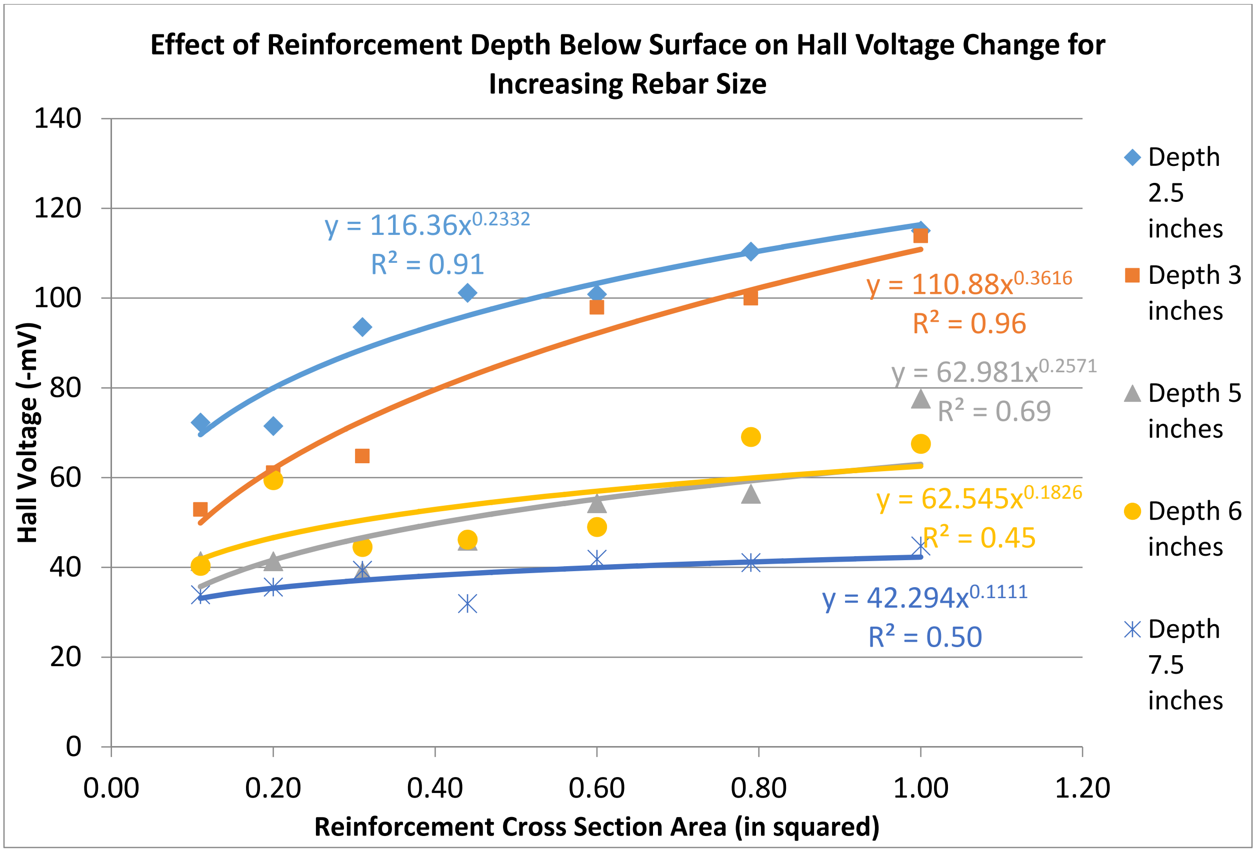

Figure 3.57: Magnetic flux leakage influence with depth.

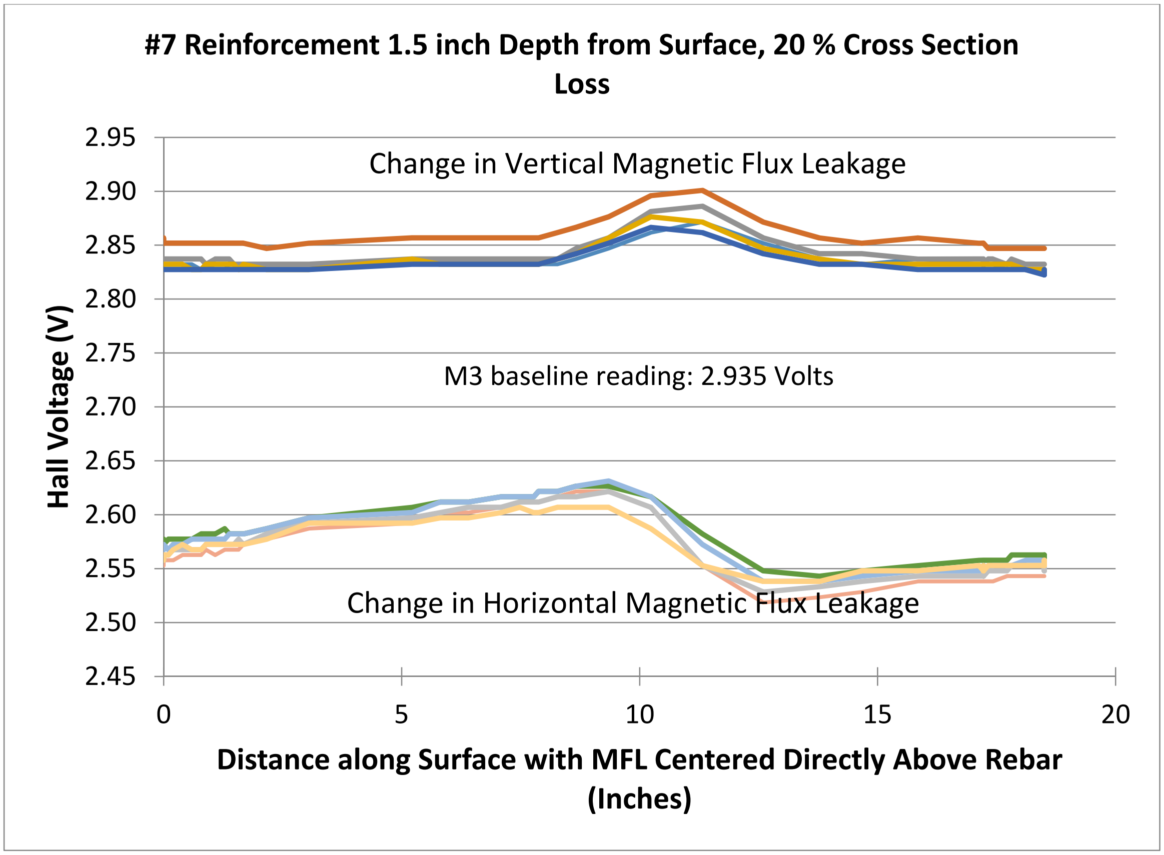

Figure 3.58: Graph of voltage change for each depth

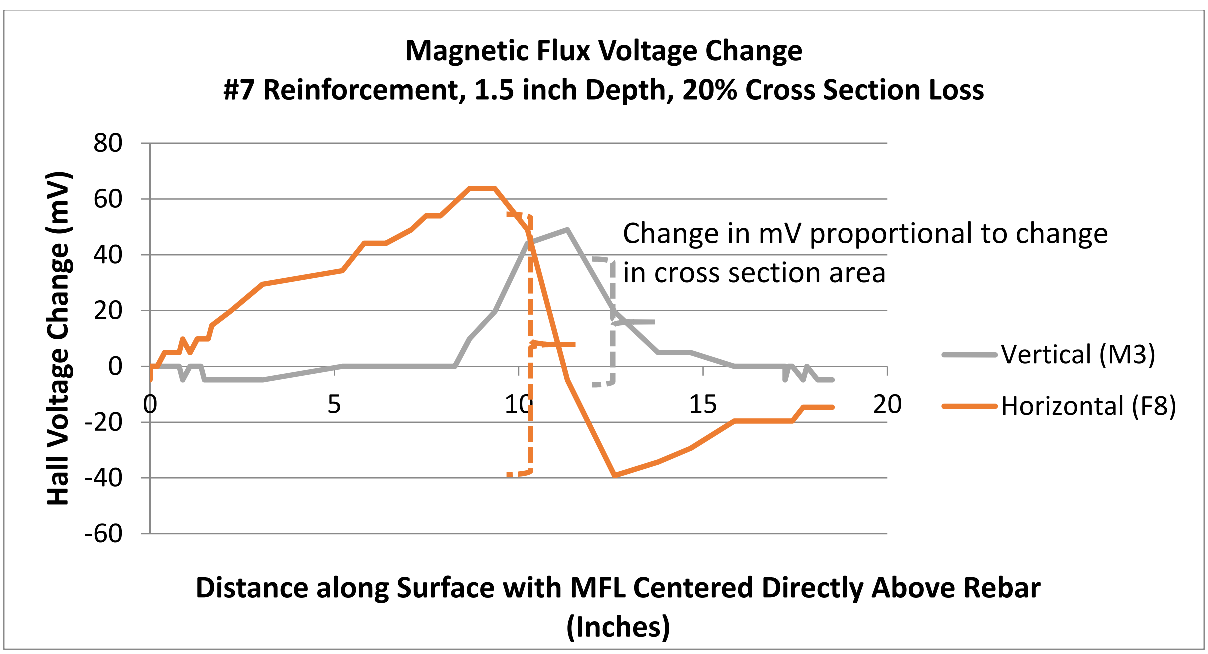

Figure 3.59: Graph showing effect of 20% loss